Effects of Irreversible Electroporation and High-Frequency Irreversible Electroporation for the Treatment of Breast Cancer

Sofie M. Saunier

Thesis submitted to the Faculty of the

Virginia Polytechnic Institute and State University

in partial fulfillment of the requirements for the degree of

Master of Science

in

Biomedical Engineering

Rafael V. Davalos, Chair

Irving C. Allen

Scott S. Verbridge

May 4th, 2023

Blacksburg, Virginia

Keywords: Electroporation, Irreversible Electroporation, High-Frequency Irreversible Electroporation, Breast Cancer, Triple-Negative Breast Cancer

Effects of Irreversible Electroporation and High-Frequency Irreversible Electroporation for the Treatment of Breast Cancer

Sofie M. Saunier

ACADEMIC ABSTRACT

Breast cancer (BC) is the second most common cause of cancer-related deaths for women in the United States, estimated to affect 1 in 8 women. Difficulties arise in BC treatment due to the hormone sensitivity and heterogeneity of the malignancies, and the poor prognosis after metastases. Due to the immense physical and psychological effects of conventional surgical methods, minimally invasive, non-thermal, focal electroporation-based ablation therapies are being investigated for the treatment of BC. Irreversible Electroporation (IRE) delivers a series of long, monopolar electrical pulses via electrodes inserted directly into the targeted tissue which disrupt cellular membranes by creating nano-scale pores, killing the cells via loss of homeostasis while promoting an immune response. However, IRE requires cardiac synchronization and a full-body paralytic to mitigate unwanted muscle contractions, which motivated the creation of second generation High-Frequency IRE or H-FIRE. H-FIRE delivers short, bipolar pulses to destroy cancer cells without muscle contractions and nerve excitation, and allows for more tunable treatment parameters. Throughout my thesis, I discuss investigations of H-FIRE for the treatment of triple-negative and hormone-sensitive BC cell lines and compare efficacy to IRE outcomes. To further establish the translation and understanding of H-FIRE for BC applications, my master's thesis focuses on: (1) determining the lethal electric field threshold of both cell lines in a 3D hydrogel matrix after H-FIRE and IRE; and (2) employ those values in a single bipolar probe numerical model to simulate *in vivo* treatments. The culmination of this thesis advances the use of H-FIRE in breast tissues, as well as demonstrates how *in vitro* data can be used to develop clinically relevant numerical models to better predict *in vivo* treatment outcome.

Effects of Irreversible Electroporation and High-Frequency Irreversible Electroporation for the Treatment of Breast Cancer

Sofie M. Saunier

GENERAL AUDIENCE ABSTRACT

Breast cancer (BC) is one of the most deadly forms of cancer for women in the United States, affecting every 1 in 8 women. Difficulties arising in the treatment of BC include the hormone sensitivity of malignancies, metastatic tendencies, and the diversity of the tissue that characterizes the breast. Surgical options like mastectomy or lumpectomy are most often used when treating BC; however, these are incredibly taxing on the patient. This reason has sparked investigations of focused ablation modalities for the treatment of BC, specifically non-thermal mechanisms like electroporation-based therapies. Electroporation explains the phenomenon that cells subjected to a high enough electric field will result in increased membrane permeability, allowing for the entrance of therapeutic agents in reversible mechanisms, or cell death beyond an irreversible point. Irreversible Electroporation (IRE) has shown success for the treatment of prostate, liver, kidney, and pancreas. However, due to some drawbacks, second generation High-Frequency IRE (H-FIRE) is increasingly being investigated for certain cancer types and is the main focus of this thesis project. Within this thesis, I discuss investigations of H-FIRE with applications to treat malignant breast cell lines. Specifically, my thesis focuses on: (1) determining the point at which cancer cells damage is irreversible; and (2) incorporate those values into a numerical model used to simulate electroporation treatment if a tumor were embedded in a layer of fatty connective breast tissue. The culmination of this thesis enhances our understanding of H-FIRE in the breast, with the hopes of future transition of application into animal studies and ultimately the clinic.

This dissertation is dedicated to all of those have supported me along this incredibly fulfilling yet challenging journey to obtain my master's degree. To both of my parents, thank you both for your unrelenting support throughout my time in graduate school. You are always so eager to learn more about what I've been working on and making sure that I'm not too stressed while assuring me everything will be okay. I'm eternally grateful for the sacrifices you both make on a daily basis to make my life easier, and to make sure that I have no worries besides my schooling. You are both my role models, and I know that Gwen and I are so very lucky to have such amazing parents like you. Dad, I watched you battle IPF for many years, and come out the other side of a double-lung transplant with such commitment to your health and your family. You are an inspiration to me every day, and a constant reminder that I can get through anything. My passion for biomedical sciences always comes into play whenever I have the opportunity to help you with injections or medicines, and even years of seeing you with tools and building sparks the engineering passion inside me. You are a huge part of my interest in this field, and I'm so thankful for your constant commitment to my success. Mom, thank you from the bottom of my heart for the work you put in to make my life as easy as possible. You came to the States alone with nothing and your incredible work ethic has gotten you so far in life. I can only hope that I inherit this quality from you, and I am able to give my children one day the same amazing experience you have given me. To my sister, thank you for making Blacksburg feel like my second home. I know I can always come to you with any of my worries and you'll be there to listen to me with open arms. You (and Lilly) have been so important to me during this journey, and I am forever thankful to have a sister like you. To my brother, while you may not have been down here on Earth to verbally push me further in life, I never forget that I have a guardian angel constantly looking over me as a big brother would. You have inadvertently taught me how to be the big sibling and take care of Gwen, but part of me will always be the middle child. We miss you so much. I love you all.

Acknowledgments

Firstly, I would like to acknowledge my advisor and mentor Dr. Rafael V. Davalos. Thank you for your generous wisdom and insight into my thesis project over the last two years. It has been a true pleasure to be a member in your prestigious lab, working alongside so many extremely talented and intellectual students; I am incredibly humbled and honored to be included within this group of researchers. Your contributions to the biomedical engineering field are astounding and inspiring, and it has been a pleasure working under your wing learning about electroporation. You have always pushed me to do my best, work my hardest, work collaboratively with my fellow lab mates, and taught me not to be discouraged when confused. I am very thankful for your interest in my academic career and efforts in helping me pass each hurdle I face.

I'd also like to thank my committee members, Dr. Irving Coy Allen and Dr. Scott Verbridge for the guidance and mentorship I've received throughout my masters. To Dr. Allen, it has been my pleasure working with you for almost two and a half years in undergrad and I am so grateful we were able to continue collaborating throughout my graduate degree. It was in your lab where I first got to learn the basics of cell culture, as well as become equipped with handling rodents which quickly became my favorite aspect of research. I learned so much from the histotripsy and cholangiocarcinoma project with Dr. Vlaisavljevich, in which I was encouraged and challenged to play a key role in both the mechanical engineering and immunological sides of the project. I've also had the pleasure of taking an immunology class with you which I got to learn a lot about a field I'm interested in. I look forward to keeping in touch with you and continuing to see the amazing work you do. To Dr. Verbridge, thank you for being available for any questions regarding my thesis ideas and research topics I've

been curious about. I've also thoroughly enjoyed having you as a professor and getting to learn more about the cancer field from you. Your neighboring lab space has provided numerous equipment necessary to performing my experiments, and your lab members have always been willing to donate a helping hand.

To the BioElectroMechanical Systems Lab, thank you so much to every single one of you for playing such a major role in helping me become the researcher I am today. Each of you have pushed me to succeed and are always available to help me answer my research questions. To Sabrina N. Campelo, thank you for being my initial mentor in the lab, and introducing me to electroporation. I find you to be such an inspiration with all of your incredible accolades, and I know you will go so far in life. To Nastaran Alinezhadbalalami, Kenneth Aycock, Edward Jacobs, Josie Duncan, Zaid Salameh, Kailee David, Julio Arroyo-I want to thank each and every one of you for your constant support and uplifting energy that has gotten me through the roughest parts of this journey. You are all not just my colleagues but friends too, and I can't wait to watch each of you grow and discover new things in the biomedical engineering field.

I would also like to thank the Virginia Tech-Wake Forest School of Biomedical Engineering and Sciences, for allowing me to take part in such a program that enabled me to pursue my goals and be surrounded by the best peers. I would also like to acknowledge support from the Institute for Critical Technology and Applied Sciences (ICTAS) and the Center for Engineered Health (CEH) in Kelly Hall at Virginia Tech.

Contents

List of Figures

List of Tables

List of Abbreviations

BC Breast Cancer

EFT Electric Field Threshold

EP Electroporation

ER Estrogen hormone receptor

H-FIRE High-Frequency Irreversible Electroporation

HER2 Human Epidermal Growth Factor 2

IRE Irreversible Electroporation

PR Progesterone hormone receptor

RE Reversible Electroporation

TMP Transmembrane Potential

TNBC Triple-Negative Breast Cancer

Chapter 1

Background and Introduction

1.1 Breast Cancer and Alternate Therapies

Breast cancer (BC) remains one of the deadliest forms of cancer and is the second most common cause of cancer-related deaths for women in the United States [20]. Although the death rate has been steadily decreasing since 1992, the rate of new cases of BC in women accounts for one third of all new cancer cases [2, 4, 86]. Variation in incidence rate between ethnic background is also present, as BC remains the highest cause of death for African American and Hispanic women [20]. Typically, lumpectomies and mastectomies are most often chosen for tumor resection due to the certainty of complete tumor cell removal as well as lower chance of metastases when removed at the appropriate stage. The difference between these two procedures is that a mastectomy will remove the entire breast tissue in addition to some nearby lymph nodes to ensure the cancer hasn't spread, whereas a lumpectomy aims to preserve the breast, and only removes the distinct lump and some portions of the lymph nodes. While these conventional methods remain the most popular among physicians, there is an immense toll that breast removal takes on the human body both physically and psychologically.

BC can be characterized by certain genetic factors that allow clinicians to better determine high-risk patients based on their hereditary components. Two tumor suppressor gene mutations in the BRCA family (BRCA1 and BRCA2) account for 40% of familial BC cases

[84], but the cumulative risk of developing BC for a person 80 years or older that has the BRCA1 mutation is 80% [36]. A women's risk of developing BC increases as they age, even without a BRCA gene mutation. If a women tested negative for a BRCA gene mutation but someone in their family did, they would have the same risk of developing BC as someone who tested positive for the abnormal gene but had no family history. Research is currently being conducted to discover new BC susceptibility genes and learn more about familial risks. Breast tumors caused by the BRCA1 gene mutation are also typically characterized by a triple-negative phenotype, where the tumor lacks the three receptors commonly found in BC: the estrogen hormone receptor (ER), progesterone hormone receptor (PR), and the human epidermal growth factor 2 (HER2) receptor [28]. Breast tumors can range in their expression of these receptors. Breast endothelial cells are regulated by the endocrine system, which is responsible for regulating hormone production. Estrogen for example, mostly released by the ovaries, is essential in controlling endothelial cell proliferation and differentiation [11]. Triple-negative breast cancer (TNBC) is an extremely aggressive variant, which represents 15% of invasive BCs, and is associated with a poor prognosis with a low five-year survival and high recurrence rates [28, 84]. Due to its lack of all three receptors, TNBC is also extremely difficulty to treat. In order to gain a consensus on how hormone receptors affect response to treatment, it is necessary to treat a multitude of phenotypically different BC cell types. Table 1.1 compares currently available treatment methods for BC. The treatments fall under either surgical, non-thermal focal or systemic, or thermal focal ablation modalities. Majority of the focal ablation modalities have been used as conjunctive therapies in addition to surgery; however, these are growing as individual treatment options today. Thermal ablation modalities are not ideal for many cancerous tumors as this mode of treatment draws heat into the surrounding vasculature leading to a possible incomplete ablation and thrombosis within the blood vessels. As well, thermal ablation denatures proteins intra- and extracellularly near the target site which causes a loss in functionality. General anesthesia required for

most procedures can cause adverse short- and long-term side effects in patients, as well as be costly for those that are uninsured. The outpatient constraint is defined as being able to receive the treatment without being admitted to the hospital or without having to stay for monitoring anywhere from 2-24 hours post-treatment. The development of scar tissue at the surgical site inhibits follow-up surgical visits, hindering post-treatment progress analysis. In general, preserving healthy, non-cancerous tissue is the overall goal for any cancer therapy, but some of the discussed treatment methods don't achieve this.

Based on patient and tumor qualifications, there are other standard treatment options typically associated with BC. Radiation is commonly used in conjunction with a lumpectomy procedure but requires weekly routine hospital visits and may cause undesirable side effects including hair loss, swelling, and breast tenderness [69]. Chemotherapy is also a well-known treatment for various types of cancers; however, these toxic drugs are dispersed throughout the patient's entire body with the hopes of killing any cancer cells that spread from initial tumor site. These agents can cause a slew of side effects including hair loss, fatigue, infection, fertility complications, or neuropathy [3]. Research shows that some chemotherapies can elicit a positive immune response by triggering both innate and adaptive immunity via subverting immunosuppressive breast tumor mechanisms or inducing immunogenic cell death [17]. Although chemotherapy can target metastasis scattered throughout the body, chemotherapeutics are not always able to directly target the entire primary tumor site.

Common targeted drug agents, like tamoxifen and raloxifene, are used to treat ER+ BC subtypes, but few research has shown success for treating TNBC [30]. While immunotherapy is also considered a plausible treatment for BC, it can be grouped into a form of targeted drug therapy, since some immunotherapeutic drugs are used to target specific proteins. Immunotherapy drugs work by enhancing the body's natural immune reaction by eliciting a positive immune response to try to fight the immunosuppressive breast tumor microenvironment. Hormone therapy is another BC treatment option designed to target one or more of

the receptors, either preventing hormone production or blocking the effects of the hormone driving cancer growth. However, hormone therapy can only be used for breast tumors that are hormone sensitive, and typically must be used in conjunction with another therapy.

Focal ablation modalities that rely on thermal energy to ablate malignant tumors capitalize on their minimally invasive capability to achieve better cosmesis than invasive techniques. These include high-intensity focused ultrasound (HIFU) which emerged in the 1940s, cryoablation in 1967, radiofrequency ablation (RF) in 1975, and microwave ablation in 1990. HIFU causes protein denaturation and coagulative necrosis as ultrasound waves propagate through tissue at high frequencies leading to increases in temperature [75]. No skin incision is required which is why it's considered a non-invasive procedure; however, it does require a medium to pass through due to the differences in attenuation between air and water or skin, which is why ultrasound transmission gels are used in ultrasound applications. Duration of treatment for HIFU is very long, lasting between an hour or more than two hours [74], which would need to be reduced to be widely used in clinical practices. Some research has shown that HIFU can generate a positive immune response, but the thermal mechanism of cell death may potentially have deleterious effects on ensuing immune stimulation [12]. While HIFU has been studied in the context of BC, a HIFU imaging platform dedicated to BC still needs to be developed to achieve positive outcomes [35]. Cryoablation works by employing extremely cold thermal temperatures in repeated protocols of freezing and thawing to destroy cancerous tissue. Cryoablation's systemic antitumor immune response has significantly contributed to its potential for benefit in the clinic [75]; however, further research still needs to be done to optimize treatment techniques. RF ablation uses inserted electrodes under ultrasound guidance to employ alternating radiofrequency current waves to generate heat and destroy malignancies. RF ablation seems to be a promising modality due to safety measures and complete ablation rates [105]; however, there is not enough data to suggest this option promotes a positive anti-tumor immune response and clinical trials to

determine treatment efficacy for BC still remain [68]. While relatively new to the field of focal ablation, microwave ablation uses electromagnetic waves to thermally ablate tumors and has demonstrated promise for the treatment of cancer, but further research needs to be conducted for this technique to be widely accepted. Additionally, microwave ablation cannot be used to treat breast tumors that are larger than five centimeters in diameter, inhibiting it's application for late-stage metastatic breast tumors [101].

Table 1.1: Comparison chart for currently available treatment methods for breast cancer. +/- indicates both possibilities dependent on treatment application.

Type of Treatment	Treatment	Outpatient	Minimally Invasive	Non-thermal	No general anesthesia /paralytic	Targets/removes entire tumor	Antitumor immune response	Does not form scar tissue	Preserves healthy tissue
Surgical	Mastectomy	+/-		✓		✓			
	Lumpectomy	✓	✓	✓		✓			✓
Non-thermal Focal	H-FIRE	✓	✓	✓	✓	✓	✓	✓	✓
	IRE		✓	✓		✓	✓	✓	✓
	Radiation Therapy	✓	✓	✓	+/-	+/-	+/-	+/-	
Non-thermal Systemic	Targeted Drug Therapy	✓	✓	✓	✓		✓	✓	✓
	Hormone Therapy	✓	✓	✓	✓		+/-	✓	✓
	Chemotherapy	✓		✓	✓		+/-		
Thermal Focal	HIFU		✓			✓	+/-		
	Cryoablation		✓			+/-	✓		
	Radiofrequency (RF) Ablation	✓	✓		+/-	+/-	+/-		
	Microwave Ablation		✓			✓	+/-		

Currently, vast improvements are being made to current cancer therapies. The biomedical engineering field plays a key role in this, as developments to newer, innovative tumor ablation modalities have shown efficacy over the last decade. Combinatorial strategies that utilize the advantages of focal ablation modalities plus additional drug adjuvants are providing improvements for BC treatment. Of note, electroporation (EP)-based modalities are of peak interest, as this technology can be applied to various cancer types with successful tumor reduction. Specifically, irreversible electroporation (IRE) and second generation high-frequency irreversible electroporation (H-FIRE) will be of focus in this thesis for the

treatment of BC. H-FIRE is the only treatment option that capitalizes on all the advantages for an optimal treatment option compared to standard surgical procedures and newer focal ablation modalities. IRE is currently not considered an outpatient procedure due to the full body paralytic requirement to mitigate muscle contractions, alluding to the need for clinical development of H-FIRE applications for BC. Although uncommon, there are some cases of minor scarring post-IRE treatment in kidney and prostate applications [43, 51], which can lead to poor circulation, decreased function, or general pain around the site. This further elucidates the importance of accurate treatment planning for electroporation delivery within the breast.

Chapter 2

Electroporation

2.1 Theory

Electroporation explains the phenomenon that cells exposed to an external electric field increases the lipid membrane permeability via disruption of the cellular membrane [97, 98]. Although the discovery of electroporation dates back more than half a century ago [87], details into the mechanisms behind the biophysical phenomenon didn't begin to accumulate until the late 1970s. The transient change of membrane permeability due to electroporation was detected by Neumann and Rosenheck, in which catecholamines (monoamine neurotransmitters), were released as a result of the induced electric fields in a vesicular model system [67]. Ultimately, modeling the membrane lipid system became of great interest, and motivated further studies of developing mechanisms for membrane-based electroporation [48].

It is critical to understand the theory behind cellular electroporation in order to optimize said mechanism for biomedical applications. The potential distribution associated with an electrical pulse surrounding a spherical cell with a nonconducting membrane in an external applied electric field, $\vec{E}$, can be described by the Laplace equation:

$$\nabla \cdot (\sigma \nabla \Phi) = 0 \tag{2.1}$$

where Φ is the electric potential and σ is the electrical conductivity of the tissue, and has the following solution for the transmembrane potential (TMP):

$$TMP = f \cdot E \cdot r \cdot cos(\theta) \cdot (1 - e^{\frac{-t}{\tau}}) \tag{2.2}$$

where

$$\tau = r \cdot C_m \cdot (\frac{1}{\sigma_i} + \frac{1}{2\sigma_e}) \tag{2.3}$$

$$f = \frac{3\sigma_e[3d_m r^2\sigma_i + (3d_m^2 r - d_m^3)(\sigma_m - \sigma_i)]}{2r^3(\sigma_m + 2\sigma_e)(\sigma_m + \frac{1}{2}\sigma_i) - 2(r - d_m)^3(\sigma_e - \sigma_m)(\sigma_i - \sigma_m)} \tag{2.4}$$

where f is the form factor describing the cell's impact on the extracellular field distribution, r is the radius of the cell, and θ is the angle between the location on the cell membrane where TMP is measured and the direction of the applied electric field $\vec{E}$. Equation 2.2 is also known as the Schwan equation, which gives insight into the transmembrane potential induced by an external electric field applied to a spherical cell [91]. The external electric field triggers an increase in the TMP, and if this exceeds a critical threshold, structural defects in the phospholipid bilayer will allow ions and macromolecules to permeate the cellular membrane. Equation 2.3 gives the solution to the membrane charging time constant τ (1 μs or less) determined by the specific membrane capacitance per unit area C_m, and σ_i and σ_e (intracellular and extracellular conductivities respectively.) [29, 55, 90]. In Equation 2.4, f [mV/(V/cm)] is a coefficient used to exhibit the influence of cell packing density; in other terms, the relation of cell packing density to cell separation distance [48]. Explicitly, σ_i, σ_m, and σ_e are the conductivity of the cytosol (intracellular), membrane, and extracellular fluid within a cell, respectively. The thickness of the cell membrane is given by d_m, with r still being the cell radius. Through many *in vitro* experiments, f simplifies down to 1.5 in Equation 2.2 for a perfectly spherical cell, assuming a completely electrically insulative lipid bilayer ($\sigma_m \approx 0$) [7, 19]. The Schwan Equation can also be solved as a steady-state function,

which does not include the $(1-e^{\frac{-t}{\tau}})$ term in Equation 2.2 [52]. This steady-state equation is used for direct current (DC) applications to determine the induced transmembrane voltage for a single spherical cell [53]. As can be seen in the top schematic in Figure 2.1, with the blue line simulating a perfectly spherical cell, the TMP will be highest if the direction of the applied electric field is closest to 0°, since the cosine of zero is 1. However, if the electric field is applied closer to 90° to the cell, then the TMP is theoretically zero. The bottom schematic in the figure illustrates the outcome of TMP in relation to electric field, form factor, and cell size, which heavily influence the TMP equation (Equation 2.2). Higher form factors are typically associated with more complex and elongated cells, which resultingly increase the TMP [10, 82]. The lowest possible form factor value is 1 which represents a circle [82], although we assume a form factor of 1.5 for spherical cells in the context of electroporation [7, 19]. This highlights the importance of comparing *in vitro* and *in vivo* electroporation results, as cells are more spherical and smaller while in suspension, but will become larger and stretched out *in vivo*, as is the case for cells embedded in 3D collagen hydrogel matrix that mimic their *in vivo* morphology (see Chapter 3). In this example, the TMP for cells in collagen (simulating an *in vivo* response to treatment), will be higher than the same cells in suspension, due to the larger cell size. With a higher TMP is becomes more likely to induce cell death from electroporation, i.e. it is easier to kill the cells. Therefore, electroporation is more effective for larger cells, which will have a lower electric field threshold as a result. Diving further into DC versus AC (alternating current) fields, the form factor (f) and the cell size (r) still impact the TMP; however, the exponential time component in Equation 2.2 will also affect the TMP, as well as the density of pores formed [47]. As can be seen in Figure 2.2, there is expected to be a higher TMP with larger pulse widths and with more elongated cells, which confirms the trend between cell size and TMP. Cell permeability is also shown in Figure 2.2, where the amount of pores per area is higher at larger pulse widths and larger cells because of the larger amount of available surface area.

Weaver and Mintzer [99], who based their conclusions off studies by Litster [57, 92] exploring the stability of spontaneous pore formation on membranes, proposed a mechanism for membrane rupture during electroporation based on energy levels during such event. They found that the free energy available for pore formation is dependent on both the applied electric field and membrane properties. In this model:

$$\Delta E(R, U) = 2\pi R \cdot \lambda - \pi R^2 \cdot (\sigma + \alpha U^2) \tag{2.5}$$

ΔE is the free energy required to create a pore with radius R, λ is the tension of the edge line of the membrane, σ is the surface tension of the membrane, and a is a value selected to represent the contrast of the dielectric contents in that of water and membrane lipid. From this equation we can estimate the pore formation rate, which is further described in detail in [76, 93, 98]. The incorporation of both the applied external electric field and the intrinsic physical properties of the membrane in this model is advantageous since surface and line tension have been shown to influence the outcome of electroporation [49]. Although the field of electroporation has been studied for many years now and there is a consensus of the pore formation process, there is still a lack of information regarding how the membrane recovers [54, 98]. As of right now, we know that there are two possible explanations for cell death: permanent membrane lysis or loss of homeostasis in which contents of the cell are lost prior to resealing [48].

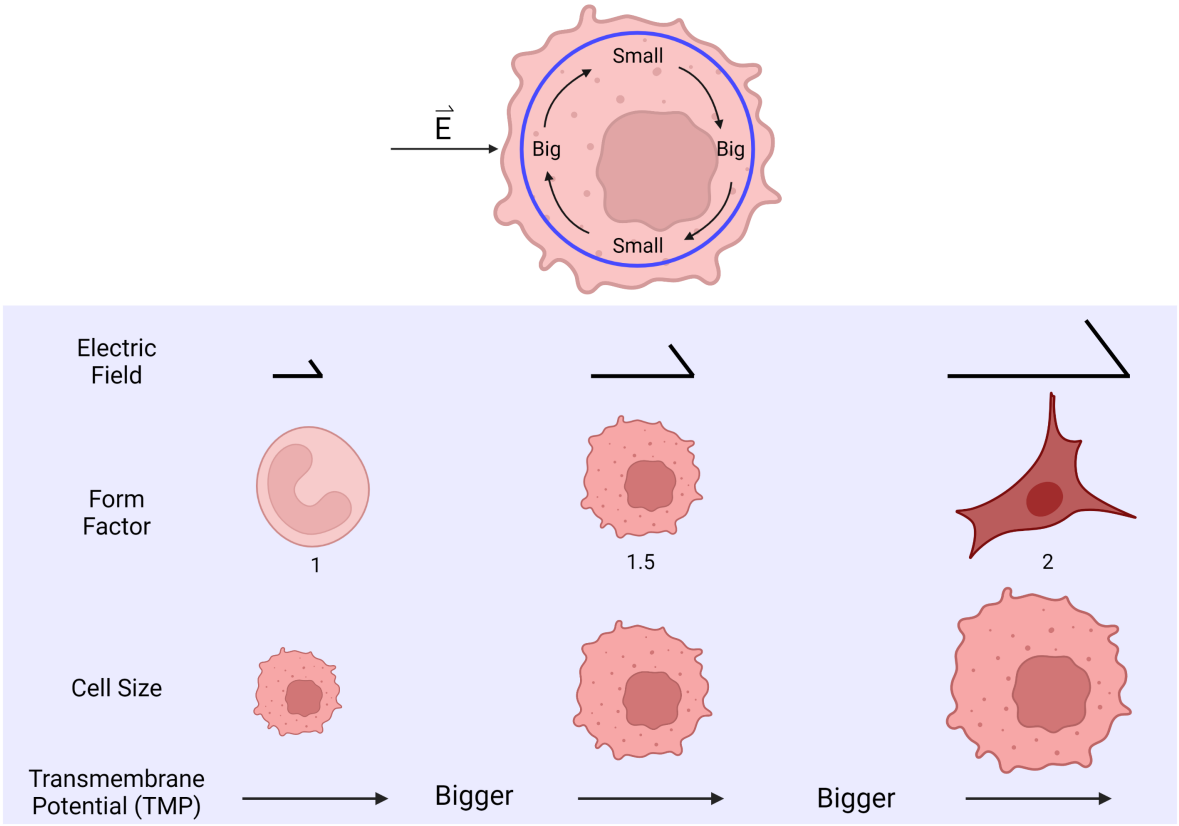

Figure 2.1: Transmembrane potential (TMP) is dependent on direction (angle) of applied electric field, electric field magnitude, and cell size. The TMP will be greatest if the field hits the cell at 0° but smaller if the field contacts the cell at 90°. As the cell size increases, the electric field and TMP will both increase. Figure created with BioRender.com.

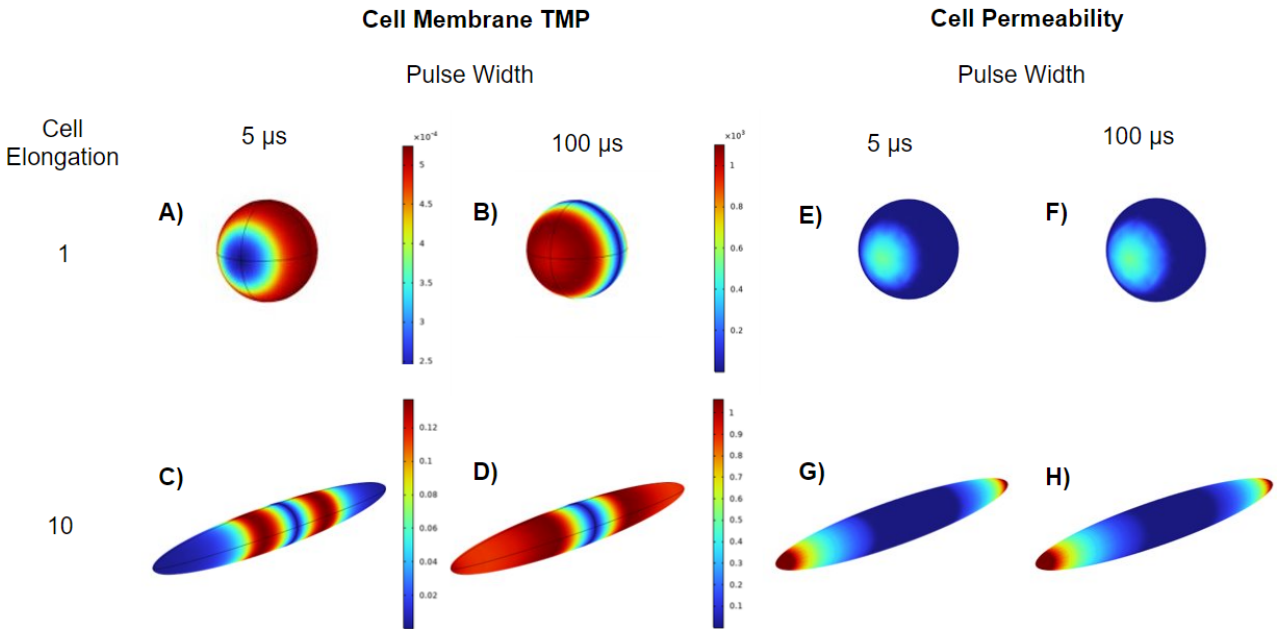

Figure 2.2: TMP and cell permeability change depending on cell elongation and pulse width. (A-D) 3D images of cell membrane TMP for 5 μs and 10 μs pulse widths and two cell elongation scenarios show changes in TMP depending on pulse width and cell size. Legends to the right correspond to each respective figure. (E-H) 3D images of cell permeability (pore density) for the same scenarios show little changes.

2.2 Electroporation-based Therapies for Cancer

2.2.1 Literature Review

Electroporation was first observed for its ability to breakdown cell membranes via applied electricity in the 1950s [87]. Soon after this, other physical applications of the principle were used in molecular biology for gene transfection, food sanitation by inactivating bacteria in the 1980s, and in newer clinical practices for increased drug uptake, tissue ablation, and gene therapies. Many of these applications utilize the phenomenon's ability to temporarily permeabilize the cellular membrane to allow the influx of certain agents into the cells, after which the formed pores can reseal with that desired agent in place. This process is termed reversible electroporation (RE) which may also sometimes be referred to as electropermeabilization or electrotransfection, and has been developed for use in other applications. In the early 1990s, the most common application of RE, electrochemotherapy (ECT), was created. This therapy capitalizes on the increased permeability of the cellular membrane to help cells intake large cytotoxic chemotherapy drugs, which are otherwise intravenously injected to travel systemically throughout the body. ECT has been tested with various chemotherapeutic drugs, namely bleomycin and cisplatin, with the ability to use lower drug concentrations and inhibit off-target toxicity levels [7, 18, 60]. ECT has shown success in clinical trials for liver cancer [32], pancreatic cancer [46], and brain cancer [81]. Another popular RE application includes electrogene transfer (EGT), also known as gene electrotransfer or DNA electroporation, which aims to directly inject plasmid DNA into cells to transfer desired genetic material. This application is being heavily investigated in laboratory settings through transfection assays, but clinical applications are still being developed; however, some active clinical trials are exploring the use of EGT for HPV, HIV, pancreatic, prostate, lung and skin cancers to name a few. Electrofusion or cell-to-cell fusion is another application of RE

mechanisms, used for creating immune-enhancing therapies or fusing protoplasts of plants [39, 94]. Additionally, electroimmunotherapy utilizes the combination of irreversible electroporation mechanisms with immunomodulatory drugs [39]. The shared benefit between all EP-based therapies is that they don't rely on thermal strategies to ablate tumors, which can be a major drawback depending on the tissue type as the advantage of non-thermal mechanisms is the ability to preserve surrounding structures by minimizing thermal damage. Research is continually being performed with EP-based modalities, such as microfluidic applications like utilizing electroporation to try to permeabilize the blood brain barrier of brain endothelial cells [16]. In 2005, Davalos et al. was the first to explore the concept of irreversible electroporation (IRE) to ablate tissue without additional cytotoxic drugs [25]. Combinatorial EP strategies have been investigated, such as using IRE and ECT for glioma treatment [62]. In this study, Neal et al. tested the effectiveness of IRE pulsing protocols with the addition of two chemotherapeutic drugs bleomycin and cisplatin through *in vitro* experiments. They found that the combination of ECT with IRE increased cytotoxicity and therapeutic ablation volume by 2.1-2.3 times compared to IRE alone [62]. IRE has gone on to become a well-established tumor treatment option for a variety of tissue types.

2.2.2 Irreversible Electroporation

Irreversible electroporation is a minimally invasive, non-thermal modality, that can deliver rapid treatments while sparing vasculature and critical nerves, inducing a local and systemic positive immune response [56]. This application can be verified with imaging and be used to treat unresectable tumors. Blood perfusion will hinder thermal ablation modalities like radiofrequency ablation because thermal modalities are reliant on tissue contact [51, 78], but IRE can be used to treat tumors that are near large vasculature due to it being unaffected by heat sink. A characteristic IRE waveform can be seen in Figure 2.3A, in which a single

100 μs monopolar pulse is delivered at a frequency 1 Hz. Finite element modeling can be used to design IRE treatment protocols that are confined to the desired area by visualizing the electric field distribution within the tissue by incorporating tissue properties [34].

Since its first proposition in 2005 [25], IRE has shown success in numerous *in vivo* and clinical studies for the lung, kidney, brain, prostate, pancreas, and liver. Neal et al. [66] characterized prostate tissue *in vivo* to predict the lesion area after IRE and determined the lethal electric field threshold to be 1072 $\pm$ 119 V/cm. Tissue characterization experiments are required to determine the necessary preliminary electrical parameters needed for future treatment modeling. In another study by Neal et al. [65], the authors investigated IRE for kidney ablation at three different voltage-to-distance ratios. This paper also focused on comparing numerical modeling methods (static, linear dynamic, and asymmetrical sigmoid dynamic) to see which most accurately correlated to lesion size and electrical properties. A lethal electric field threshold of 575 $\pm$ 67 V/cm was determined. The asymmetrical sigmoid dynamic conductivity function was the most accurate and precise, but the simpler linear dynamic model also matched predictions [65]. The NanoKnife system, which includes a generator and electrode probes, has been used to safely ablate a variety of tumors with IRE. In a study by Rossmeisl et al. [80], the system was used to treat intracranial gliomas in dogs. Median survival for all treated dogs was 119 days, and the 14-day post-treatment Karnofsky Performance Scale score (health score) was 80 on a scale of 60-90 which improved from the dogs' scores prior to treatment [80]. A validated perfused organ model was used by Bhonsle et al. [14] to characterize IRE ablations in pig livers, perfused with phosphate-buffered saline to maintain viability. This study aimed to provide a means to avoid animal trials for investigating IRE results while maintaining reliability and consistency. It was found that ablation dimensions in the perfused organ model matched *in vivo* ablations, and provided consistent IRE trends as the ablation dimensions grew with increasing pulse number [14]. Another study further elucidated the effectiveness of IRE for liver ablation with an internally cooled

electrode to reduce tissue temperatures and electric current, improving treatment outcomes [70]. While still in its preliminary stages, IRE is being investigated as a treatment option for cardiac ablation [88].

Neal et al. [63] was the first to investigate the feasibility of IRE for treating BC. Through *in vitro* experiments, a lethal electric field threshold of 1000 V/cm for the MDA-MB-231 cell line was determined, and further modeling was done with this value to simulate BC treatments. This 3D model showed that electrodes were placed within the targeted tumor near the peripheral tissue. Three different simulations with varied conductivity ratios were run to see the effect on the electric field distribution within the model. This feasibility study sparked an interest in further investigating the potential of IRE for the treatment of BC. A follow-up study by Neal et al. [64] developed the first *in vivo* clinically relevant model for IRE for BC. A single needle electrode geometry was used to treat orthotopically implanted BC tumors (MDA-MB-231 cells) in female mice. This study used the same lethal electric field threshold of 1000 V/cm as previously determined to treat the tumor. Tumor regression was seen in five out of the seven treated mice compared to consistent growth in control groups, proving IRE successful in treating tumors in the mouse mammary fat pad [64]. Another study by Goswami et al. [42] was interested in studying the relationship between various pulse parameters on cell signaling and immune-cell trafficking, as the immune response is a very important factor in cancer treatment and progression. By performing *in vitro* experiments on a TNBC cell line with varied electric field strength and exposure time (number of pulses), they found that thymic stromal lymphopoietin signaling, which can drive pro-cancerous immune cell phenotypes in BC, was downregulated above a certain threshold independent of exposure times. They proposed that more studies are warranted to further investigate IRE's potential anti-tumor immune response [42]. A group at Purdue University has also been investigating IRE effects through *in vitro* cuvette experiments with various human and mouse BC cell lines (MCF-7, MDA-MB-231; 4T1), looking into changes in cell

viability after varied treatment parameters [44, 77]. Other studies from the same group have investigated the combination of enzyme inhibitors (galloflavin) with electroporation [41] and assessed quantitative proteomics to understand the biological response to EP treatment [40]. Thermal dissipation is an important consideration during electroporation treatment planning, as the resulting Joule heating can lead to thermal damage nearby critical structures. Although Joule heating can be a potential result of IRE treatments, it does not use thermal energy as the primary mechanism of cell death, unlike HIFU or RF ablation as previously mentioned. With correct thermal mitigation strategies, irreversible EP mechanisms are capable of ablating tissue without damaging non-cellular structures. Because of this advantage, IRE can be used around major blood vessels [7]. While not discussed in detail here, temperature considerations and thorough thermal mitigation strategies have been studied and can be referred to in [9, 24, 26, 27, 37, 71].

Although proven successful in *in vitro* and *in vivo* animal models, there are serious drawbacks that inhibit IRE from certain cancer types in clinical settings. For instance, the long monopolar pulses that are characteristic of IRE (Figure 2.3A) lead to undesirable electrochemical effects such as changes in pH or electrical arcing. Electrical arching has been documented to occur when too high of an electric field is applied, converting water to gas causing the electric pulse to travel through air. IRE also requires cardiac synchronization with ECG to prevent arrhythmia, as well as a neuromuscular paralytic and general anaesthesia to avoid unwanted muscle contractions from nerve excitation during treatment. Due to these reasons, IRE requires further research to be feasible for clinical application for patients with BC.

2.2.3 High-Frequency Irreversible Electroporation

Due to the disadvantages of IRE, a second-generation mechanism termed High-Frequency Irreversible Electroporation (H-FIRE) was created, using shorter pulses to better predict

tissue ablation as opposed to longer monopolar pulses [5]. This minimally invasive application maintains many of the positive attributes of IRE, in addition to minimal muscle contractions, negligible electrochemical effects, having a more consistent field distribution and ablation shape, mitigating impedance changes, having potential inherent selectivity to malignant tissue phenotypes, and not requiring cardiac synchronization or full body paralytic [5, 15, 33, 45]. However, due to the shorter pulses, H-FIRE typically requires a higher voltage to generate the same amount of cell death as IRE. With proper treatment planning, H-FIRE is capable of destroying all of the targeted tumor, but will not form scar tissue, and has been shown to promote a positive immune response [79].

H-FIRE splits the long IRE monopolar pulse (Figure 2.3A) into a burst of shorter, biphasic pulses. An H-FIRE waveform (Figure 2.3B) is constructed as: positive phase (pulse width anywhere from 1-10 μs), followed by an inter-phase delay (1-5 μs), a negative phase – the same magnitude as the positive, and finally ended with an delay between pulses (1-50 μs). This single bipolar burst of pulsed electric field is repeated until a desired energized time (typically 100 μs) is reached. Preliminary studies have established the feasibility of H-FIRE across multiple electrode geometries and organs of interest. DeWitt et al. [31] tested a single needle electrode plus a grounding pad approach for delivering H-FIRE in an *in vivo* porcine experiment for liver tissue. No adverse effects were observed, and this study illustrated the ease of a single needle/grounding pad setup as opposed to a multiple electrode geometry in difficult anatomical regions. O'Brien et al. [72] utilized this single-needle approach to demonstrate feasibility in an *in vivo* porcine model for pancreatic cancer and found that average ablation volume increased as the pulse width increased (i.e., area for the 1-5-1 waveform was smaller than the area for the 5-5-5 waveform). The group also found specific lethal electric field thresholds for pancreatic cancer at each specific waveform; again, demonstrating the feasibility of H-FIRE for tumor ablation without the need for intraoperative paralytic agents or cardiac synchronization. Siddiqui et al. [85] utilized the application

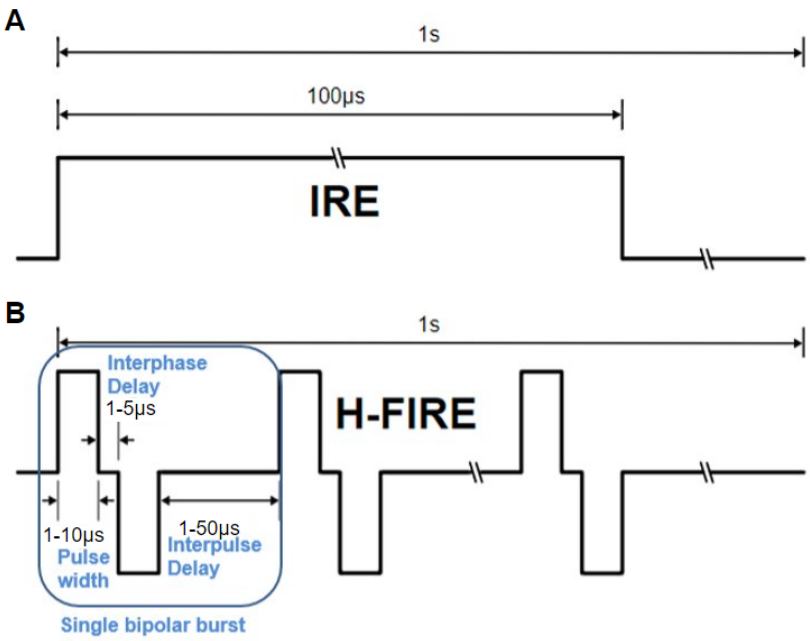

Figure 2.3: Depiction of IRE (A) and H-FIRE (B) waveforms.

for liver tumors in a porcine *in vivo* model to test H-FIRE's ability to induce reproducible and effective ablation zones with a two-needle configuration. The authors demonstrated a less than five-minute-long treatment time was needed to achieve reproducible ablation areas across pulse numbers 100, 200, and 300. No EKG abnormalities were noted in the pigs during treatment, and the authors were able to discern apoptotic cell death regions at pulse number less than 200 compared to necrotic tissue at larger pulse numbers [85]. H-FIRE is also being explored as an avenue for brain malignancies. Murphy et al. [61] specifically investigated biological cell death mechanism dynamics after H-FIRE treatment for primary and metastatic malignant brain tumors through *in vitro* cell experiments. The authors were able to characterize H-FIRE-induced cell death and recovery by choosing appropriate treatment parameters and pulsing protocols, as they found that at high enough H-FIRE doses the application can inhibit damaged cell recovery, alluding to H-FIRE's therapeutic potential. A huge therapeutic approach for brain malignancies is targeting the blood brain barrier (BBB), a natural network of tightly dense blood vessels and tissue designed to keep harmful

substances from reaching the brain. Lorenzo et al. [59] varied pulse widths and interphase delay in H-FIRE waveforms, as well as electrode configurations, to understand their role in potential BBB disruption and ablation volume. Through *in vitro* and *in vivo* rodent experiments, the authors demonstrated that optimizing treatment parameters is crucial and has the potential to modulate cell death while also inducing target ablation volumes. The first human clinical trial of this application was done in 2018, where H-FIRE was used to treat prostate cancer in 40 men without the incorporation of cardiac synchronization [33]. Four weeks post-treatment, all patients had completely preserved urinary and sexual function and no cardiac-related side effects were observed, which demonstrated the effectiveness of H-FIRE treatment.

As far as utilizing H-FIRE for the treatment of BC, seldom work has been done to investigate this. However, some researchers have piqued interest in using the application for investigating immunological responses. Ringel-Scaia et al. [79] wanted to specifically understand the immune system activation following H-FIRE treatment. Therefore, a well established 4T1 mouse breast tumor model was used where mice where subjected to a 2-5-2 H-FIRE waveform for 200 bursts and 100 μs of on-time. They found that H-FIRE can kill BC cells via inflammatory modes of cell death necrosis and pyroptosis, as well as shift the anti-inflammatory tumor microenvironment to pro-inflammatory ultimately inducing a systemic anti-tumor immune response. It was also found that local H-FIRE treatment reduced the number of metastatic lesions in mice with intact immune systems, which may be another reason for optimizing H-FIRE for breast applications as 20-30% of BC is will become metastatic. There is still a lack of information regarding variation in H-FIRE parameters and their subsequent treatment outcomes, as well as testing the application with human BC cell lines and in a clinical setting.

2.3 Overview and Thesis Hypothesis

Through various preclinical studies, IRE and H-FIRE have shown success for many forms of cancer. While IRE has been studied various times in the context of BC *in vivo* [63, 64], H-FIRE has yet to be established as a conclusive treatment option besides efficacious proof in a rodent model [79]. Breast tissue is naturally heterogeneous, consisting of connective adipose (fat) tissue, ducts, and lobules or the glands that produce milk. Due to these biological challenges, there is motivation for extensive numerical modeling which would allow engineers to help improve treatment planning and clinicians' understanding of treatment outcome depending on where the tumor is situated in the breast. This thesis focuses on utilizing H-FIRE for the treatment of BC by changing various treatment parameters across two phenotypically different human BC cell lines in order to explore H-FIRE as a possible therapeutic option. The purpose of this thesis is to show that we can perform *in vitro* experiments and obtain critical data that can be used in clinically-relevant numerical models to accurately simulate treatment planning and ablation volume *in vivo*. In the future, this work can also help facilitate pre-clinical *in vivo* animal experiments which would be more relevant to human clinical trials of H-FIRE for BC.

Chapter 3

Experimental Validation of High-Frequency Irreversible Electroporation for Breast Cancer

3.1 Abstract

EP-based modalities have been efficacious as alternatives to standard of care treatments in a variety of tumors. Currently, there is a paucity of information regarding the use of H-FIRE for the treatment of BC, providing movitation for these studies. Here, *in vitro* hydrogel experiments were performed for two human malignant breast cell lines to determine the electric field thresholds (EFTs) from ablation volumes post-treatment and compared between cell lines and waveforms. Lethal EFTs for the MCF-7 cells were 540 V/cm for 5-1-5, 473 V/cm for 10-1-10, and 405 V/cm for IRE. Lethal EFTs for the MDA-MB-231 cell line were 1824 V/cm for 5-1-5, 1674 V/cm for 10-1-10, and 1574 V/cm for IRE. These trends fit the expected results that as pulse width is increased, EFT will increase. While ablation volumes were calculated for the MDA-MB-231 cells, the reliability of the results remains questionable. However, the overall results demonstrate the potential of H-FIRE to treat specific BC cell lines, with the aim of translating results to future *in vivo* studies.

3.2 Introduction

This chapter aims to experimentally validate the use of H-FIRE for the treatment of BC across two different malignant cell lines. The two cell lines used in these *in vitro* experiments were MDA-MB-231 and MCF-7 human malignant breast cell lines. The MDA-MB-231 cells are a highly metastatic TNBC line harvested from an adenocarcinoma. This cell line is considered very aggressive and difficult to treat, but is heavily used in research when studying a triple-negative phenotype. MCF-7 cells are considered slightly less aggressive and ER+, meaning it is sensitive to estrogen through the estrogen receptor alpha within the cytosolic membrane, representing the most common subtype of BC, luminal A [102]. This subtype of BC is characterized with positive expression of the hormone receptors but negative expression of HER2. The MCF-7 cell line has shown varied dependence on the progesterone receptor (PR+/-) but is not dependent on the human epidermal growth factor 2 (HER2-). Therefore, the MCF-7 line comprises various individual phenotypes which differ in gene profile and receptor expression [11]. These phenotypically different BC cell lines provide useful *in vitro* BC models by representing different hormone receptor characteristics. The 3D cell-embedded collagen scaffold used in these experiments allows for a more realistic model for treatment as cells will maintain their *in vivo* morphology. These *in vitro* platforms are used to optimize pulse parameters and determine the EFTs across multiple cell lines and waveforms from a single experiment. This advantage is critical in electroporation studies, as comparing cell characteristics allows us to understand differences in irreversible threshold [6]. No changes in conductivity allows us to superimpose the Laplace equation (Equation 2.1) to determine electric field thresholds.

Two previous studies by Neal et al. [63, 64] investigated the use of IRE for treatment of malignant breast cells. Firstly, they demonstrated the feasibility of the technique for treating MDA-MB-231 cells *in vitro*, in which they determined a baseline electric field threshold that

can kill the cells, and optimized a numerical model to best simulate treatment response *in vivo*. A follow-up study orthotopically injected the same cell line into female mice and applied electroporation treatment, resulting in significant tumor reduction with a clinically relevant single needle bipolar electrode design. Besides in an *in vivo* study with a malignant murine cell line, no investigations have been comparing treatment outcome of H-FIRE to IRE for malignant human breast cell lines. We hypothesize that with appropriate treatment parameters and waveforms, we can achieve more desirable ablations *in vivo* for H-FIRE compared to IRE. The data presented supports the use of H-FIRE as a treatment method for heterogeneous BC, but also highlights similar outcomes for IRE. Therefore, further treatment tuning is required to prove H-FIRE more successful than IRE for breast applications.

3.3 Materials and Methods

3.3.1 Cell culture

The human TNBC cell line MDA-MB-231 (ATCC) was thawed and maintained in a T175 flask with Dulbecco's Modified Eagle's Medium (ATCC) supplemented with 10% fetal bovine serum (FBS) (R&D Systems) and 1% penicillin-streptomycin (Life Technologies) by volume. This is an adherent epithelial cell line from an adenocarcinoma within the mammary gland belonging to a 51-year-old white female (ATCC). MDA-MB-231 cells were passaged at 90-100% confluency with a 1:10 dilution ratio. The ER+, PR+/-, and HER2- human BC cell line MCF-7 (ATCC) was maintained in a T75 flask with Minimum Essential Medium Eagle (Sigma) supplemented with 20% FBS (R&D Systems) and 0.1 mg/mL human recombinant insulin (Sigma-Aldrich). These epithelial cells are treated as both a mixed adherent and suspension cell line, isolated from metastatic adenocarcinoma breast tissue of a 69-year-old

white female (ATCC). The passaging steps were the same for this cell line; however, floating cells were gently centrifuged at 120 rcf for 8 minutes and the pellet was resuspended in fresh media and put back into the plate for the first two subcultures, after which all cells became adherent. MCF-7 are characterized by circular clumps that form mounds which can be seen in Figure 3.1A, compared to spindle-shaped MDA-MB-231 cells in Figure 3.1B. MCF-7 cells were passaged at 70-80% with a 1:3 subculture ratio. For both cell lines, 0.25% Trypsin-EDTA (Gibco, Canada) solution was used for cell detachment. Cells were kept in water jacketed CO_2 humidified incubators set to 37 °C and 5% CO_2.

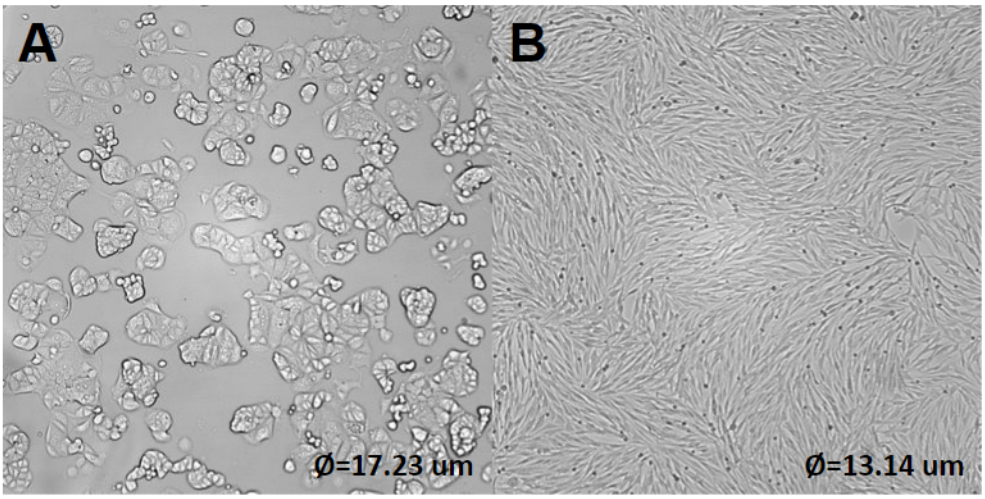

Figure 3.1: Brightfield microscope images to compare cell morphology of (A) MCF-7 and (B) MDA-MB-231 cell lines in a monolayer at target confluency (10x magnification). Average cell diameter is displayed in the bottom right hand corner.

3.3.2 Cuvette experiments - cell viability

Routine passaging steps were followed prior to cell viability experiments. A cell count of at least 1.6E6 cells/mL was required to have a cell density of 1 million cells per cuvette. After centrifugation cells were resuspended in a low conductivity electroporation buffer consisting of sucrose, glucose, basal media, and deionized water, and 600 μL of cell solution

was transferred into 4 mm electroporation cuvettes (BTX). Using a custom-pulse generator (VoltMed Inc., Blacksburg, Virginia) and a BTX 630 (Harvard Apparatus), cuvettes were treated at initial field strengths 0, 750, 1500, 2250, and 3000 V/cm with 100 bursts. Control cuvettes contained the same volume of cell solution and were placed in the electroporation chamber but no pulses were applied. After the treatment was over, the entirety of cell solution was collected and transferred to a 1.5 mL centrifugation tube (Eppendorf) and spun down at 150 rcf for 8-10 minutes. The buffer (supernatant) was removed from the eppendorf tube and the pellet was resuspended in 650 μL of supplemented media. In a 96-well plate, each cuvette was split into three wells (roughly 200 μL) to obtain three different sample readings (n=3), and left overnight in the incubator. After 24 hours post-treatment, the viability of the cells was measured through the metabolic assay AlamarBlue (Invitrogen). This common cell viability assay detects fluorometric changes of resazurin dye to its highly fluorescent form resorufin in response to metabolic activity in the cells. AlamarBlue reagent was added to each well in a 1:5 ratio of dye to media (40 μL reagent to $\sim$200 μL media). Pipetting was done to ensure complete combination, and the plate was placed on a shaker for 30 seconds while covered in foil due to the light sensitivity of the assay. The plate was incubated for two hours, after which the fluorescence was measured using a plate reader (Molecular Devices)(Ex.530, Em.600 nm). Percent viability was calculated and normalized to the untreated control groups. This data can be visualized in Figure 3.5. These cell viability experiments were only performed as an initial gauge for the MDA-MB-231 TNBC cell line, and were not repeated for the MCF-7 cells.

3.3.3 Fabrication of collagen hydrogel scaffolds

Male Sprague Dawley rat tails obtained from BioIVT (Hicksville, NY) were used for collagen extraction. After the collagen soaked in 70% ethanol, the collagen was placed in a beaker with 150 mL of sterile 0.1% acetic acid per gram of collagen. After storing at 4°C for 72 hours, collagen was placed in Nalgene centrifuge tubes (filled to 80% capacity) and centrifuged at 30,000 g for 45 minutes at 4°C. After centrifugation, the clear supernatant was transferred to 30 mL sterile conical tubes and frozen at -20°C, filled only to 20 mL. Once the collagen supernatant was frozen, the collagen was added to a container for lyophilization. Lyophilized collagen was then stored at -20°C until future use, in which the measured amount of acetic acid diluted in deionized water is added and vortexed for 20 seconds and transferred to a fridge to dissolve to achieve a final collagen concentration of 10 mg/mL (Figure 3.2). The final concentration of the collagen after everything is added is around 5 mg/mL, which is ideal for standard experimentation in the lab.

The 3D collagen hydrogel tissue mimic was constructed to investigate cell ablation area and irreversible cell death threshold in both the MDA-MB-231 and MCF-7 cells. Before experimentation, individual wells in 24-well plates were coated in high vacuum grease (Dow Corning) and sterilized under UV light for 20 minutes before plating. Once ready for hydrogel fabrication, collagen was neutralized using 10X DMEM (Sigma Aldrich) (10% of final volume) and 1N NaOH (Sigma Aldrich) (2% of initial collagen volume) until a target pH is achieved, followed by 1950 μL of supplemented media mixed with the cells. In a 24-well plate, 200 μL of cell-laden collagen was added to each well and incubated at 37°C and 5% CO_2 to allow the collagen to solidify. After 30 minutes, each well was topped with 400 µL of media and incubated for 24 hours until treatment.

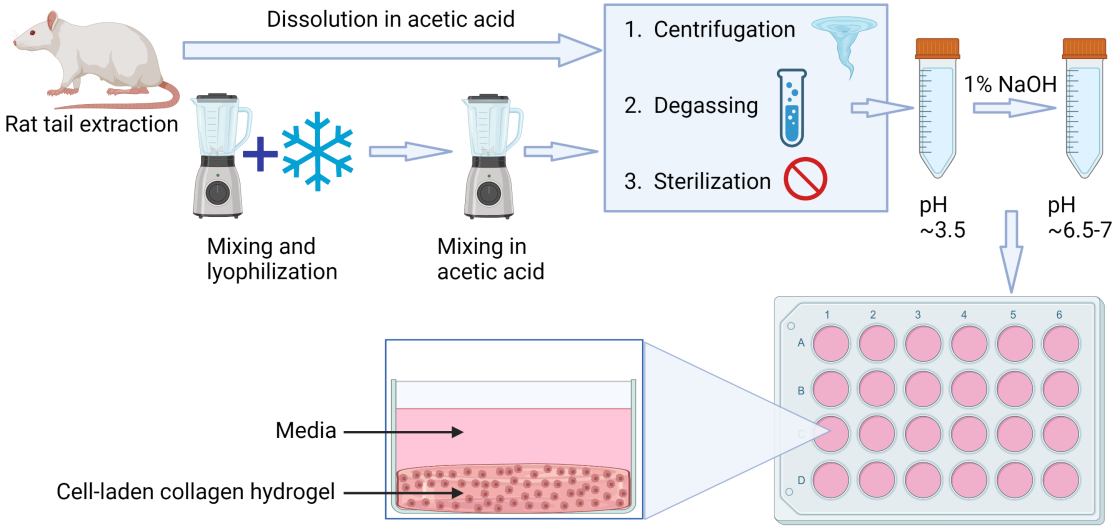

Figure 3.2: Fabrication of cell-laden collagen hydrogel scaffold. Collagen extracted from rat tails is dissolved in acetic acid, centrifuged, degassed, and sterilized through lyophilization and pH stabilized through additions of 1% NaOH. Cells added into the collagen mixture are plated, solidified, topped with supplemented culture media and incubated until treatment 24 hours later. Figure created with BioRender.com.

3.3.4 Finite element modeling

In order to back out the EFTs from the ablation volume areas obtained during the hydrogel experiments, a 3D model was made using COMSOL Multiphysics v6.1 (COMSOL Inc., Stockholm, Sweden). To simplistically model the electric field distribution for *in vitro* hydrogel studies with a two-needle electrode geometry, only dimensional parameters for the gel and the electrodes were taken into account. The collagen scaffold was modeled as a disk with a radius of 8 mm, or half the seize of an individual well in a 24-well plate, the height or thickness of the gel was 1 mm, the separation between the center of the electrodes was 3 mm, and the height of the electrodes was simulated to be 1 cm. The two-inch gauge needles (Jensen Global JG20-2.0 20 Gauge 2.0" IT Series Dispensing Tip) used in treatments were modeled with an inner diameter of 0.864 mm and outer diameter of 1.168 mm. Basic treatment parameters were also simulated in the model, like 100 μs of energized or on-time, a standard pulse rate of 1 pulse/second, 100 bursts, physiologic temperature of 37°C, and a voltage of either 600, 700, or 800 V. For a more thorough explanation as to why 800 V was eventually removed from treatments, please refer to Section 3.5. The output for the electric field distribution in the 3D hydrogel at each voltage with the two-needle electrode configuration is shown in Figure 3.3. The output data file of areas corresponding to EFTs from 0 V/cm up to 2000 V/cm was then used to match the experimental area found from fluorescent imaging with the approximate EFT to obtain lethal threshold values for the specific waveform and applied voltage. This output data can be seen in Figure 3.7.

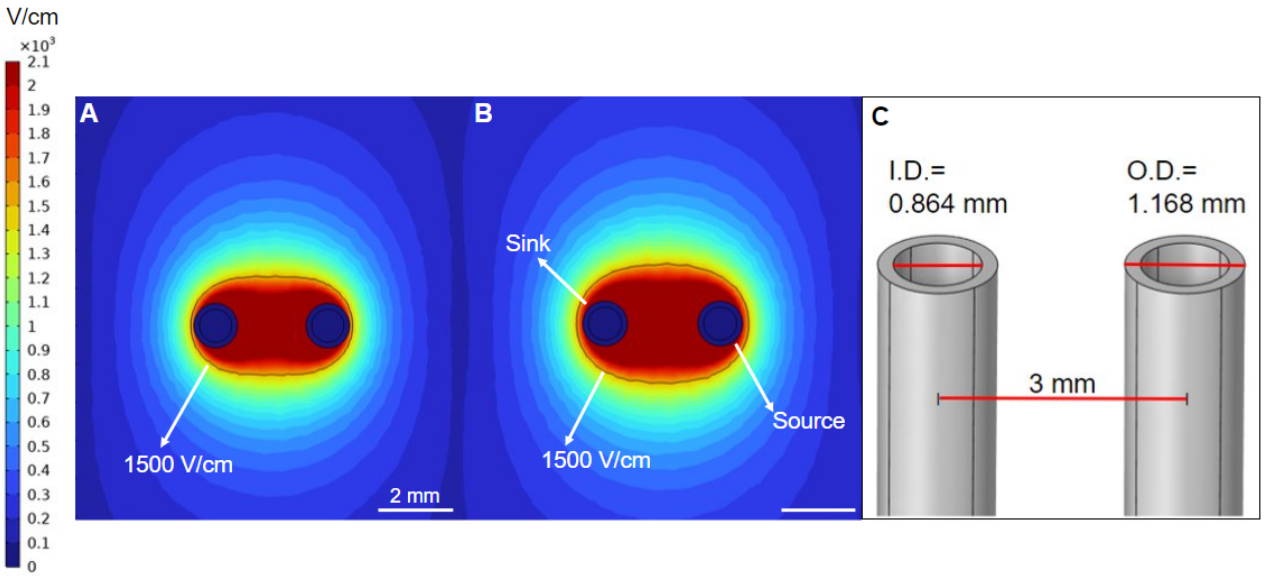

Figure 3.3: 3D electric field distribution. (A) 600 V and (B) 700 V applied between the electrodes. The black line indicates the ablation zone related to 1500 V/cm, which was the target fields based off viability experiments. As you increase the voltage, the distribution shape becomes more spherical, which will encompass more of the gel. (C) Needle dimensions (I.D.=inner diameter, O.D.=outer diameter) with a 3 mm spacing between electrodes.

3.3.5 Electroporation delivery

The electrodes and 3D printed needle holder were sterilized under UV light while a Heratherm IMC 18 incubator (Thermo Scientific, Germany) was brought to 37°C and humidified with a glass of deionized water to simulate typical incubation environment. Immediately prior to treatment, the media on top of each hydrogel was removed due to the highly conductive nature of culture media. The electroporation delivery system involves the custom-pulse generator used to deliver both IRE and H-FIRE pulsing schemes. Voltage and current were recorded using a WaveSurfer 2034z oscilloscope (Teledyne LeCroy, Chestnut Ridge, NY) with a 1000X high voltage probe (Enhancer 3000, BTX, Holliston, MA) and 10X current probe (2877, Pearson Electronics, Palo Alto, CA). Mini-grabber test clips were used to connect the electrodes to the generator in order to deliver current and voltage. The two-needle electrode holder was placed directly on top of an individual well in a 24-well plate, and the sterile hollow needles were pushed through the entirety of the gel ensuring they were both in contact with the bottom of the plate (Figure 3.4). The plate was placed inside the incubator, and treatment was applied. After which, the electrode holder was removed and 400 μL of media was added back into the well and incubated for 24 hours.

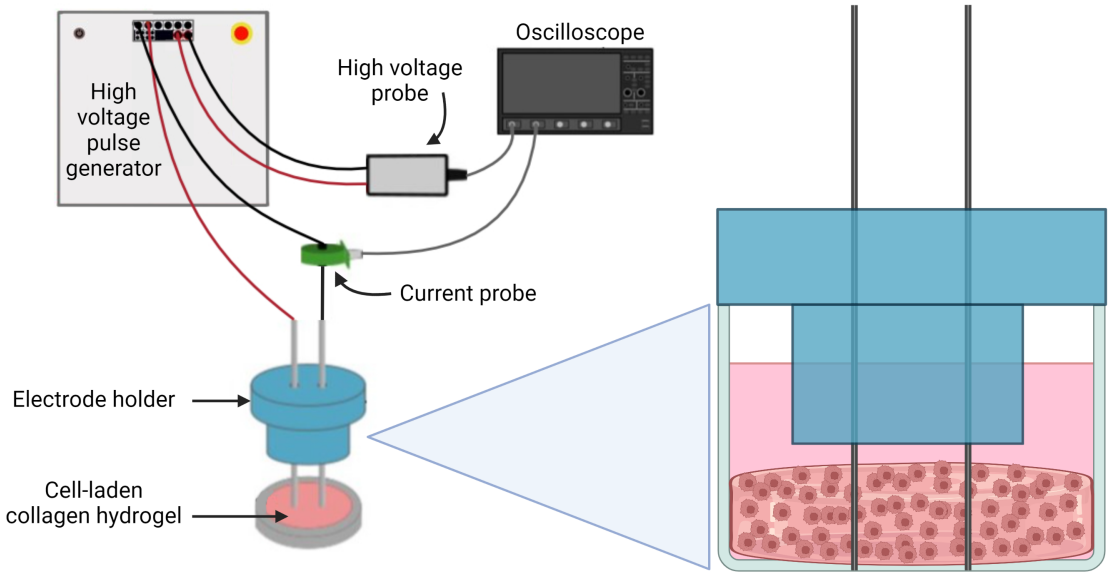

Figure 3.4: Electroporation delivery system uses a custom high voltage pulse generator, with current and voltage readings monitored during treatment via oscilloscope. Two-needle electrode configuration placed directly into the cell-laden collagen hydrogel. Figure created with BioRender.com.

3.3.6 Staining and Imaging

Following 24 hours post-treatment, plates were removed from incubation, and a stain containing phosphate buffer saline (PBS, Corning), Dimethyl Sulfoxide (DMSO, Sigma-Aldrich), Calcein AM (Invitrogen), and Propidium Iodide (PI, Invitrogen) was used to quantify live/dead cell lesion areas. Media was aspirated from each well, followed by a single PBS wash, and then 400 μL of stain was added to each treated and untreated (control) well. Once the plate was covered in foil to protect from light, hydrogels were incubated at 37°C and 5% CO_2 for 30 minutes. Thereafter, hydrogels were double washed with PBS prior to imaging using an inverted microscope (DMI 6000B, Leica Microsystems) with a 5× objective. The appropriate filters were used to image calcein AM (green; Ex:460–500; DC:505; EM:570–640) and PI (red; EX:545/26, DC:565, EM:605/70). Ablation zones were then be calculated with the Leica software by measuring area of ablation.

3.4 Results

Figure 3.5 displays the calculated viability results after an initial range of electric field strengths (Figure 3.5A) for MDA-MB-231 cells treated in electroporation cuvettes. From this, it was determined that the EFT to achieve at least 50% cell death for MDA-MB-231 cells was somewhere between 750 and 1500 V/cm. The same procedure was repeated with a smaller range of field strengths (Figure 3.5B). After these experiments, the cell death threshold to achieve at least 50% viability was determined to be approximately 1500 V/cm. Additionally, it was decided that the 2-1-2 H-FIRE waveform should be taken out of treatment protocols, as a significantly higher voltage would need to be applied to achieve similar results to other pulsing schemes. Individual data points can be seen in Table A.1 in Appendix A.

As can be seen in Table 3.1, the average EFT for the MCF-7 cell line was 540 V/cm for 5-1-5, 473 V/cm for 10-1-10, and 405 V/cm for IRE. The average EFT for the MDA-MB-231 cell line was 1824 V/cm for 5-1-5, 1674 V/cm for 10-1-10, and 1574 V/cm for IRE. Table 3.1 also displays the average ablation area (mean ± standard deviation) calculated for each waveform, which are much higher for the MDA-MB-231 cells compared to the MCF-7. For both cell lines, a sample size of six was used to generate a statistical power of 99%. An ordinary one-way ANOVA determined that the EFT was statistically different between each applied waveform ($p<0.0001$) for the MCF-7, but only one group had a statistically significant p-value of ($p<0.05$) for the MDA-MB-231. The values fit the expected trend that at lower pulse widths there will be a higher EFT, which can further be seen in Figure 3.6B and C. The main difference between the MDA-MB-231 and MCF-7 cell lines is that there was less PI uptake in the MDA-MB-231 cells, denoted by the black ablation zones in Figure 3.7A compared to the red zones in Figure 3.6A.

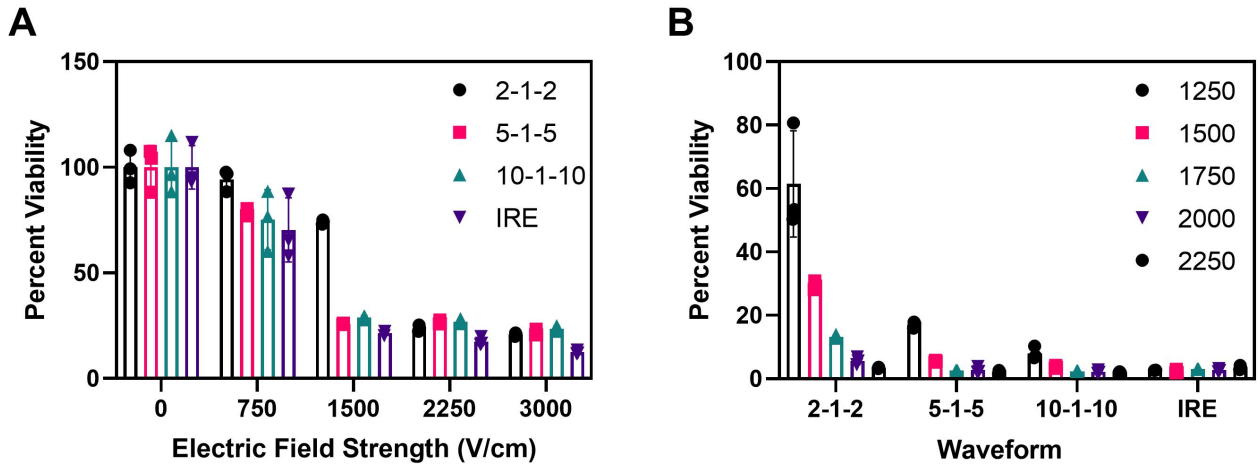

Figure 3.5: Statistical analysis for cell viability in cuvettes post-treatment. (A) Initial range of electric field strengths (0 to 3000 V/cm). (B) Additional round of experiments with narrowed electric field strengths. In all experiments three H-FIRE waveforms (2-1-2, 5-1-5, 10-1-10) and a typical IRE protocol (100 μs, 1 Hz) were applied.

Table 3.1: Experimental electrical pulsing parameters and electric field threshold data for both MDA-MB-231 and MCF-7 cell lines. In both experiments, 100 bursts were used and the energized time was matched to 100 μs. All results are presented as mean $\pm$ standard deviation.

Cell Line	Output (n=6)	5-1-5	10-1-10	IRE
MDA-MB-231	Area (mm^2)	5.69 $\pm$ 1.86	6.69 $\pm$ 2.33	7.26 $\pm$ 1.05
	EFT (V/cm)	1824 $\pm$ 173	1674 $\pm$ 211	1574 $\pm$ 56
MCF-7	Area (mm^2)	25.67 $\pm$ 0.36	29.77 $\pm$ 0.61	35.54 $\pm$ 0.36
	EFT (V/cm)	540 $\pm$ 8	473 $\pm$ 8	405 $\pm$ 4

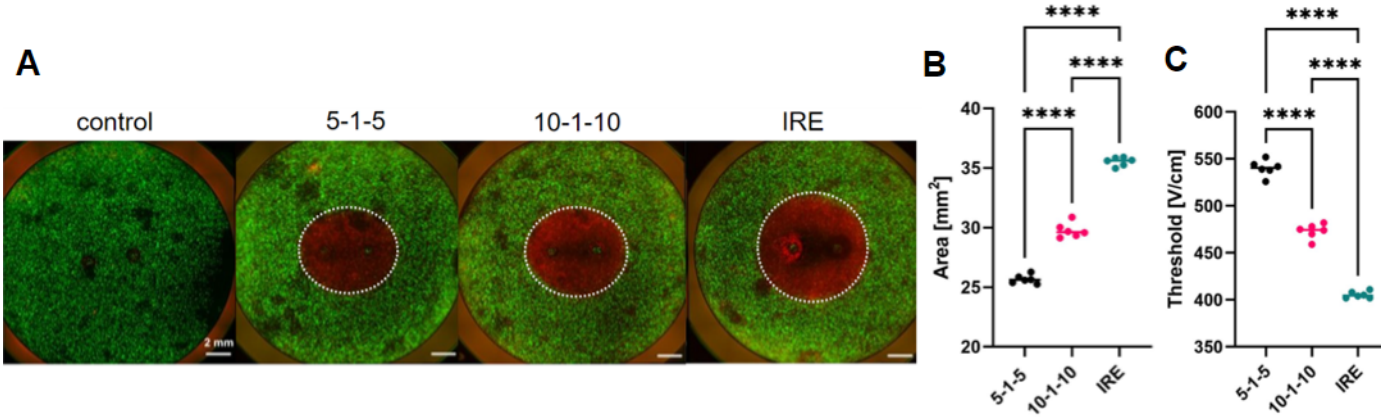

Figure 3.6: (A) Ablation areas for all pulsing schemes in the MCF-7 cells. Corresponding area measurements (mm^2) (B) and electric field threshold (V/cm) (C). Statistically significant p-values are <0.0001, demonstrating expected results with dye uptake and data analysis. Scale bars are 2 mm.

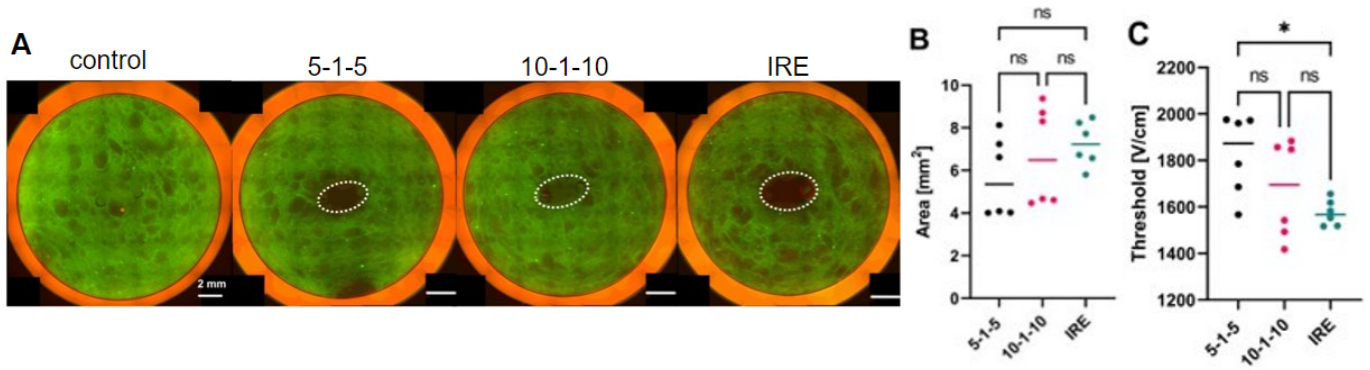

Figure 3.7: (A) Ablation areas for all pulsing schemes in the MDA-MB-231 cells. Corresponding area measurements (mm^2) (B) and electric field threshold (V/cm) (C). Statistically significant p-values are <0.05, which demonstrate that ablation did not follow expected trends. Ablation images in (A) show the lack of PI uptake within the gels. Scale bars are 2 mm.

3.5 Discussion and Conclusion

The results from these experiments provide evidence that IRE and H-FIRE have the potential to ablate malignant breast cell lines *in vitro*. Both applications demonstrated expected results in the MCF-7 cell line, in which larger ablations were seen in wells treated with IRE, followed by the 10-1-10 then the 5-1-5 H-FIRE waveforms due to the direct relationship between ablation area and pulse width. However, there is an inverse relationship between pulse width and field threshold, which explains why 5-1-5 had a higher threshold than the 10-1-10 and IRE for the MCF-7 cells.

Initially, 800 V was applied to the cells in the gels; however, consistent arching was observed, either only slightly detected from clicking at each pulse, or enough to cause the generator to stop treatment. At too high of a voltage, it is possible to melt the gel, which in turn denatures the proteins within the collagen. Initially, the goal of applying two different voltages was to yield more redundant information and more confident results to estimate and visualize the ablation zones at 1500 V/cm. However, 800 V was most likely too high of a voltage to apply in hydrogels, therefore it was omitted from further experiments and only 600 V was applied for the MCF-7 cells. For the MDA-MB-231 cells, 600 V was insufficient in generating an ablation zone, as can be seen in the data analysis in Figure 3.7B, which is why 700 V was chosen as an additional voltage to try to ablate these cells. The ablation zone images in Figure 3.7A correspond to an applied voltage of 700 V. The 600 and 700 voltages did not cause significant arching as compared to 800 V. However, in general, increasing or decreasing the voltage should not have an effect on electric field threshold, therefore the MDA-MB-231 results should be interpreted with caution.

For the fluorescent staining, PI is not permeant to live cells, but it is able to diffuse through the compromised membranes of dead cells. Once the dye is inside the cell, it binds to nucleic acids and enhances its red fluorescence upwards of 20-30-fold. Calcein AM is used to contrast

PI since it is a cell permeant dye that fluoresces green after internalization and hydrolysis by live cells. These two dyes are typically used to visualize the distinct regions within the 3D hydrogel collagen scaffold of live and dead cells after electroporation treatment under a fluorescent microscope [6]. This staining method was successful in the MCF-7 cells (3.6A), but barely uptaken in the MDA-MB-231 cells. We determined that plated cell density couldn't explain these differences, as experiments were repeated for the MDA-MB-231 cells with a density of 1, 1.5, and 2 million cells/mL whereas the target 1 million cells/mL density used for the MCF-7 was adequate. It was speculated that cell size could be a factor in dye uptake; however, there is only a relatively small difference in cell size between the cell lines, and PI is only dependent on membrane permeability and not excluded by cell size according to current literature. It was assumed that each cell line would be compatible in the 3D collagen matrix based on previous studies investigating cell invasion [13], but after comparing fluorescent images this was believed to not be the case. To investigate this possibility, 3D images of the cell-laden collagen hydrogels were taken post EP-treatment on a Zeiss LSM 800 confocal microscope using a 10× objective (Figure 3.8). These images demonstrate that MCF-7 circular cell morphology is maintained, whereas the MDA-MB-231 cells are completely degraded after being in the gel for 48 hours, as can be seen by the small cell fragments. To be sure that the dye wasn't the reason behind poor images associated with the MDA-MB-231 cells, other fluorescent dyes were also used to quantify ablation zones, as can be seen in Figure 3.9. In 3.9A, Calcein red-orange AM was used to assess cell viability by staining nonspecific esterases in live cells. Yo-Pro-1 was used in conjunction with this as it will only stain apoptotic cells. In 3.9B, ethidium bromide fluoresces dead cells red after binding to DNA by inserting itself between base pairs through intercalation [83]. Calcein AM was used with ethidium bromide to stain the live cells. Each dye stained the cells appropriately; however, it is difficult to tell what exactly is considered the ablation zone: whether it is the region directly surrounding the electrodes or spread out into the gel based

off this hazy zone. The last possibility discussed that could explain the poor MDA results was treating the cells at too high of a confluency (i.e. 90% instead of 70%). Although unlikely, other mechanical factors like the specific hormone receptors or the concentration of the collagen itself could potentially explain these differences. Further experimentation is needed before determining that the MDA-MB-231 cell line is incompatible in the type 1 collagen matrix.

Overall, we were able to achieve successful *in vitro* ablation data for the hormone-sensitive MCF-7 cell line. These experiments also helped determine the incompatibilities of the triple-negative MDA-MB-231 cells in a 3D hydrogel scaffold, which inhibits studying clinically-relevant electroporation effects to this specific TNBC cell line. In the future, it would be insightful to find such a platform that allows for realistic TNBC treatment. In the next chapter, we will utilize the electric field thresholds determined for the MCF-7 cell line only and implement them into a numerical model to examine various modeling aspects like waveform-specific electric field distribution, ablation volume and sphericity.

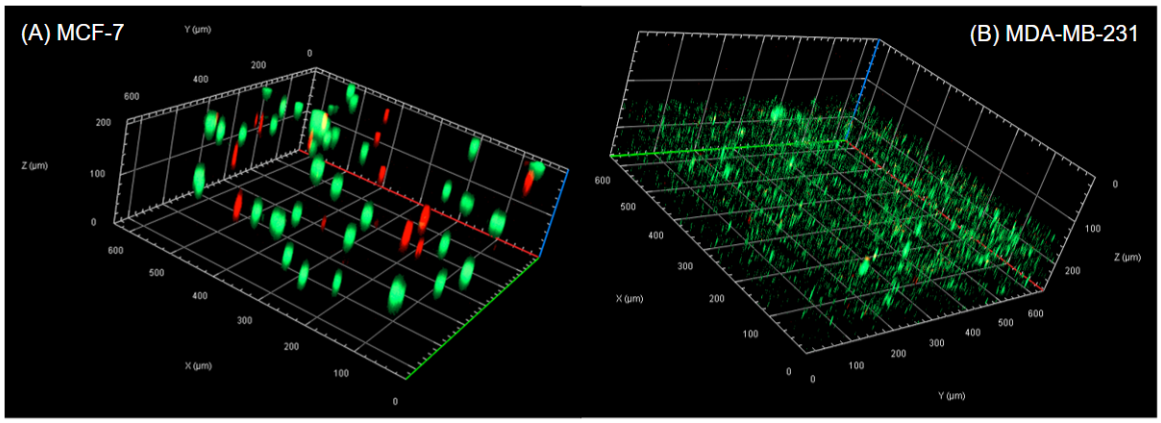

Figure 3.8: 3D confocal images of embedded (A) MCF-7 and (B) MDA-MB-231 cells in a portion of the collagen hydrogel (10x magnification). Cell morphology is maintained in the MCF-7 cells, but not in the MDA-MB-231s, alluding to their incompatibility in the collagen matrix.

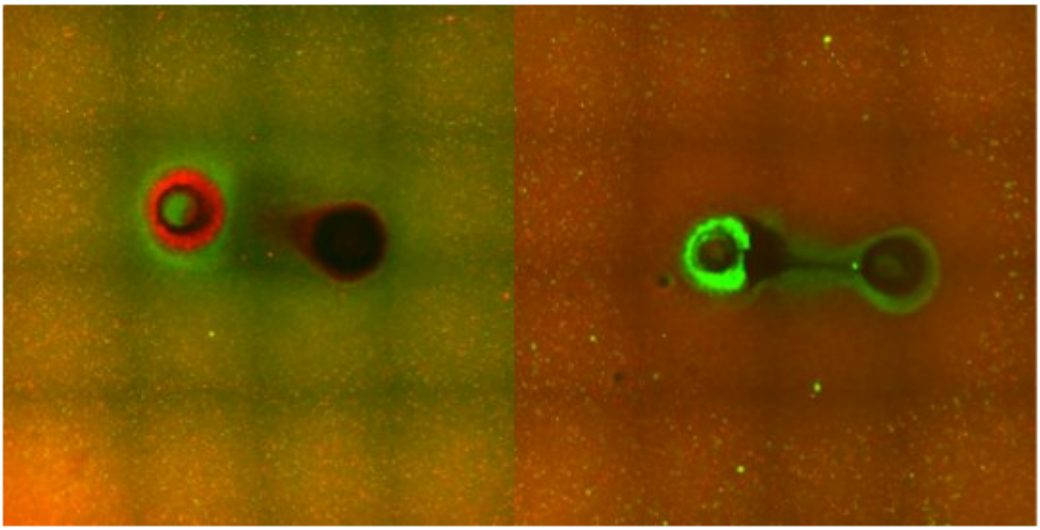

Figure 3.9: Additional fluorescent dyes properly stained the MDA-MB-231 cells. (A) Live cells are stained red with Calcein red-orange AM and dead cells are stained green with Yo-Pro-1. (B) Live cells are stained green with Calcein AM and dead cells are stained red with ethidium bromide.

Chapter 4

Implementation of experimental results in a clinically relevant numerical model of H-FIRE for breast cancer

4.1 Abstract

Prior to performing *in vivo* electroporation experiments, finite element analysis can be done using COMSOL Multiphysics, allowing researchers to study the effect of certain pulsing parameters on treatment outcome. The goal of this chapter was to investigate the comparisons between IRE and H-FIRE waveforms through relevant 2D and 3D models. The hypothesis that H-FIRE parameters can be tuned to achieve similar results to IRE was validated by performing a voltage sweep across waveforms to determine the exact voltage as which H-FIRE ablation surface area, volume, and sphericity are nearly identical to IRE.

4.2 Introduction

This chapter aims to prove how we can incorporate *in vitro* threshold results into a clinically-relevant numerical model for simulating *in vivo* treatment. Further, it was of interest in this experiment to see if we can achieve comparable ablation results to IRE by fine-tuning H-FIRE treatment parameters. COMSOL Multiphysics can tell us numerous 2D and 3D outputs that are relevant to electroporation therapy. Specifically, the software can show us electric field distribution in the target tissue, how much of the tissue is ablated, along with other visual results like thermal affects and dynamic conductivity changes. COMSOL can also tell us about joule heating, which occurs because of the resistance of current from electrical pulses traveling through the target tissue, and may result in increased electrical current since conductivity has been shown to have an effect on heat and electroporation effects. Each of these variables can be better understood through accurate numerical modeling.

Due to the incompatibilities with the triple negative MDA-MB-231 cell line, threshold data from the MCF-7 cell line was used. Although unfortunate to not be able to model the response of TNBC to EP, utilizing data from the MCF-7 cells permits us to understand EP treatment response for a luminal A subtype of BC, which is the most common form of invasive BC, accounting for upwards of 60% of BC cases [100]. Prognosis for this subtype is typically good, but treatment methods are still reliant on surgery, radiation, or chemotherapy, further motivating the need for optimizing H-FIRE treatment. We hypothesize that at the same applied voltage for all waveforms, IRE will generate a higher ablation volume than H-FIRE. However, it is also hypothesized and the main aim of this modeling experimentation, that we can tune the applied voltage in a relevant range with the H-FIRE waveforms to achieve comparable ablation volume and sphericity results to that of IRE. This experimentation aims to prove the capability of H-FIRE tuned parameters efficacious as a potential treatment option for BC.

4.3 Methods - Mathematical Modeling

Various assumptions were taken into account when designing this model. The tumor was modeled as a sphere with a radius of 1.5 cm, surrounded by a layer of healthy fatty connective adipose breast tissue with radius 3 cm. The electrodes (source and sink) both had lengths of 0.7 cm, where the insulation between them was 0.8 cm based on a commercially available electrode used by Garcia et al. [38], with a handle protruding out of the the breast being 5 cm in total length. Due to the total height of exposed electrode equaling 2.2 cm in diameter, the minimum radius of the tumor had to be above 1.1 cm to fit the entire probe. The radius of the entire probe was modeling as 0.1 cm. The stage of the breast tumor was assumed to be stage 2, or T2, which ranges anywhere from 2-5 cm in diameter and is described as localized cancer in which the mass has begun to grow and affect nearby tissue but has not yet metastasized. This stage of breast tumor was chosen due to the large number of new cases of localized BC being higher than regional (T3) or distant (T4) stages [2]. Figure 4.1 displays a 3D view of the entire numerical model with each electrode dimension described above.

Tissue characterization experiments allows us to measure voltage threshold and current values in the desired tissue, which can be correlated to conductivity. Since breast and surrounding connective tissue sections were never harvested, tissue characterization studies were not performed and various tissue parameters were pulled from literature. Some electrical and thermal properties can be pulled from the IT'IS Dielectric Properties database including electrical conductivity, density, heat capacity, thermal conductivity for the breast gland tissue (tumor mimic) and the breast fat (surrounding tissue). Suroweic et al. [89] published dielectric property values of breast carcinomas and the surrounding tissues in 1988 at frequencies from 20 kHz to 100 MHz. Initial conductivity values were extrapolated from within the manuscript with a graph-reading software to harness conductivity values of the

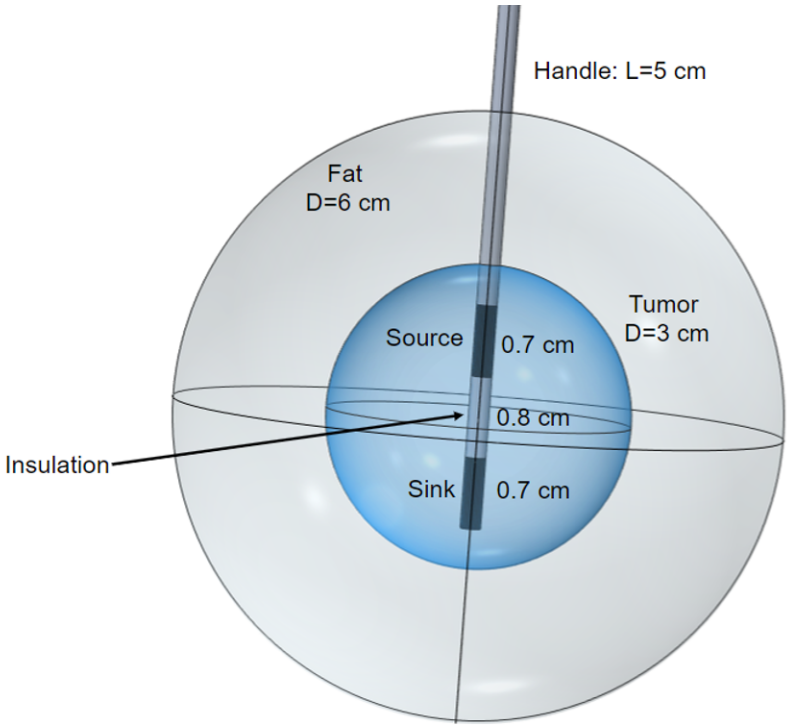

Figure 4.1: 3D view of numerical model generated in COMSOL, with the bipolar probe being inserted into the center of the tumor (blue), through the peripheral breast fat (light grey). D=diameter, L=length.

tumor (central part of the tumor) at frequencies 83.3 kHz (5-1-5), 45.4 kHz (10-1-10), and 10 kHz (IRE). Those characteristic frequencies were calculated by dividing one over the period which is the total time of a single burst (ex. period for 5-1-5-1=12) times 10^6 to be in the correct frequency range. Specific heat capacity, density, and thermal conductivity of the breast tumor and peripheral tissue were found from Neal et al. [63]. Other variables not included in Table 4.1 include blood perfusion rates, which were found to be 0.0002 $1/s$ and 0.012 $1/s$ for the fat and tumor respectively [21]. IT'IS Database was used to find the specific heat capacity and density of blood, which were 3617 $J/kg * K$ and 1050 kg/mm^2 respectively [1]. Table 4.1 contains a comprehensive list of all of the modeling parameters related to a malignant breast tumor and healthy periphery of fatty connective breast tissue pulled from the various literature sources.

COMSOL Multiphysics was used to run all of the simulated models. Model simulations are run at the intersections within a designated boundary at a user-defined mesh level. As you increase the mesh (increase the refinement), you are increasing the amount of intersections in the domain making your model more accurate. However, higher levels of mesh will take longer to run and in some cases super fine meshes may not be necessary. Therefore, a mesh convergence study was done in order to determine the optimum mesh refinement level when running the models in order to achieve maximum speed of model run-time without compromising the results. It was determined that a mesh level of 0.327 would be appropriate to run the 3D model, since this value resulted in a less than 1% difference than that of a finer mesh levels (Figure 4.2B). In the 2D axisymmetric model, a predefined mesh level of extra fine was chosen for simulations.

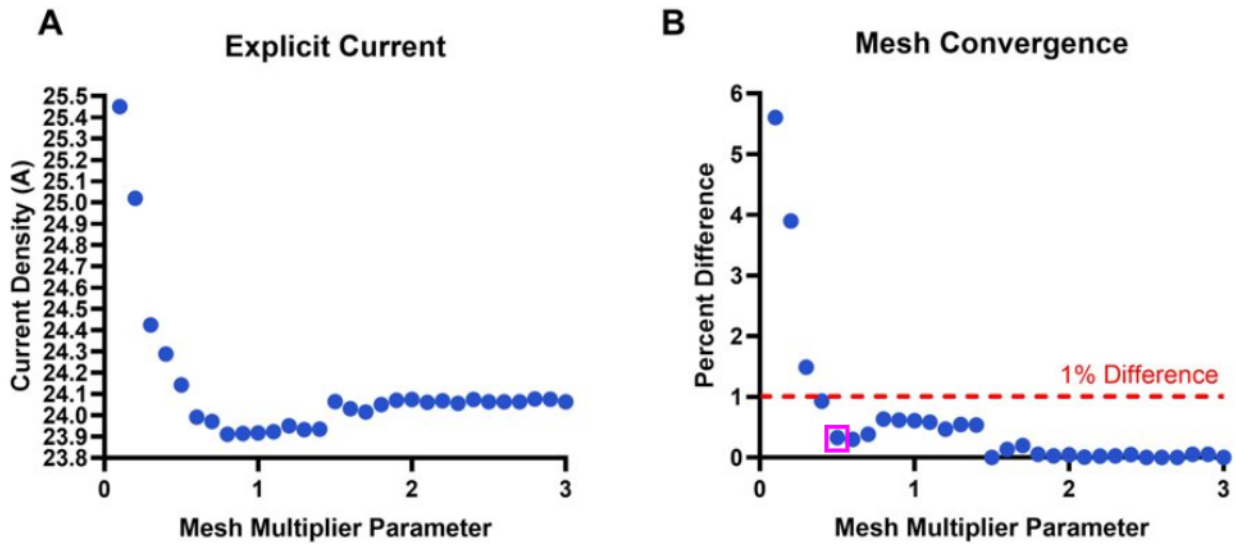

Figure 4.2: Mesh convergence study revealed a refinement level of 0.327 was appropriate for the 3D model. (A) Explicit current data across mesh levels from 0.1 (coarsest) to 3 (finest). (B) Corresponding percent difference in mesh levels. Pink box highlights chosen mesh level of 0.327.

Previous literature has demonstrated that as tissue transitions to a fully electroporated state, the conductivity of the tissue will increase and then reach a plateau [23]. This matches the

dynamic conductivity of the tissue in the model, further demonstrating that tissue conductivity is a function of applied electric field magnitude. Equation 4.1 was used in COMSOL to understand the dynamic changes in conductivity of the tumor and fat respectively:

$$\sigma(|\vec{E}|) = \sigma_0 \cdot (1 + A \cdot flc2hs(\vec{E} - E_{del}, E_{range})) \tag{4.1}$$

where σ_0 is the initial conductivity of the tissue, A is a unit less term modeled as the ($\sigma_{final,tissue}/\sigma_{initial,tissue}$-1), $flc2hs$ is the Heaviside function that is used to characterize the dynamic changes in conductivity [104], and $\vec{E}$ represents the electric field magnitude. E_{del} is treated as the electric field threshold corresponding to each waveform used during *in vitro* hydrogel experiments found to induce electroporation effects (i.e. E_{del}=540 V/cm for 5-1-5 (MCF-7)). The σ_0 and E_{del} values will change depending on the tissue selected to model was tumor or fat. Finally, E_{range} relates to the slope of the transition and was selected to be 350 V/cm based on previous studies by Zhao et al. [103]. $\sigma_{final,tumor}$ and $\sigma_{final,fat}$ were omitted from Table 4.1 because these values will not change depending on applied waveform. Based on current knowledge of the field, a cell is considered fully electroporated at 10 MHz, at which the values of $\sigma_{final,tumor}$ and $\sigma_{final,fat}$ were found to be 0.452 S/m [50] and 0.0281 S/m [1], respectively. The dynamic conductivity curve generated from the COMSOL model can be seen in Figure 4.3, which shows changes in dynamic conductivity based on the applied waveform.

Another key clinical consideration for EP treatment is the shape of the ablation. A spherical shape is more ideal than an ovular or peanut-shaped ablation as this generates a more uniform ablation. Sphericity of each ablation was calculated in order to compare the change in ablation shape depending on applied waveform. This equation can be seen in Equation 4.2,

$$\Psi = \frac{\pi^{\frac{1}{3}}(6V)^{\frac{2}{3}}}{A} \tag{4.2}$$

where V is the volume of the ablation and A is the surface area of the volume produced by the ablation, both specific to applied waveform and voltage. A volume of a perfect sphere is 1, therefore the closer the values are to 1 the more spherical the shape of the ablation.

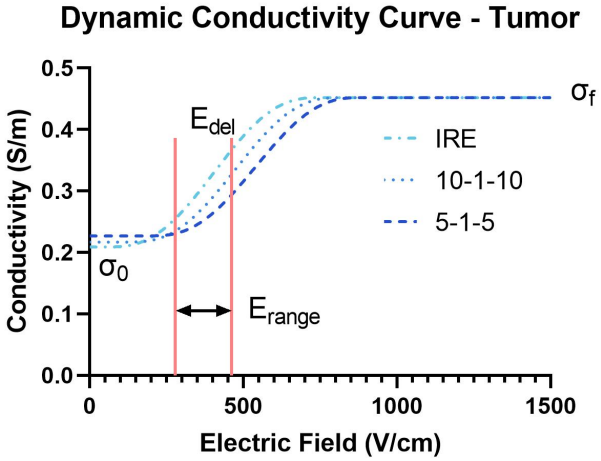

Figure 4.3: Dynamic conductivity curves for applied waveforms in the breast tumor. σ_0 is the initial conductivity of the tissue, E_{range} is half the value of on either side of the transition point (E_{del}), and σ_f is the maximum tissue conductivity after applied electroporation.

Table 4.1: Tissue properties used in numerical modeling.

Property	Variable	Value	Reference
Electrical Conductivity (S/m), 5-1-5	$\sigma_{initial,tumor}$	0.227	[89]
	$\sigma_{initial,fat}$	0.025	[1]
Electrical Conductivity (S/m), 10-1-10	$\sigma_{initial,tumor}$	0.217	[89]
	$\sigma_{initial,fat}$	0.0249	[1]
Electrical Conductivity (S/m), IRE	$\sigma_{initial,tumor}$	0.209	[89]
	$\sigma_{initial,fat}$	0.0247	[1]
Heat Capacity (J/(kg*K))	$C_{p,tumor}$	3700	[63]
	$C_{p,fat}$	3550	
Density (kg/m^3)	ρ_{tumor}	1044	[63]
	ρ_{fat}	928	
Thermal Conductivity (W/(m*K))	k_{tumor}	0.564	[63]
	k_{fat}	0.499	

4.4 Results

Figures A-C in 4.4 provide a visual depiction of the electric field distribution through the simulated breast tumor and peripheral healthy fat at the maximum clinical voltage of 3000 V. Firstly we see that the differences in electric field distributions between waveforms is very slight. In all cases, the electric field is strongest at the electrodes and dissipates outwards into the tissue, where IRE distributes farther into the tissue because of the targeted energy from the monopolar pulses. Although the H-FIRE waveforms are characteristic of higher frequencies than that of IRE, the change in polarity from H-FIRE helps to mitigate thermal effects due to electroporation, which are expected to be stronger in an IRE pulse scheme. Two domains were specified for calculating the surface area, volume, and resulting sphericity for the ablations, where V1 is the tumor and fat domains combined to encompass the entire ablation region, and V2 is the tumor only domain.

From the sphericity calculations at the maximum clinical application of 3000 V applied, the sphericity of the 5-1-5 waveform was 0.6969, 0.7135 for the 10-1-10, and 0.8169 for IRE. This demonstrates that at 3000 V, IRE will generate the most spherical ablation volume. To investigate how much of the breast tumor is being ablated for all pulsing schemes, the tumor ablation volumes can be compared to the total volume of the tumor, calculated to be 14.14 cm^3. Based off the V1 values, 5-1-5 is ablating 49.7%, 10-1-10 is ablating 65.6%, and IRE is ablating 87.5% of the simulated breast tumor. IRE also spreads into the fat more than the H-FIRE waveforms, which alludes to the desire to optimize H-FIRE treatment protocols for maximum treatment efficacy. To investigate how H-FIRE outcomes could achieve similar results to IRE, a parametric sweep was performed for each H-FIRE case to find the scaled voltage that achieved similar ablation volumes and sphericities to IRE at 3000 V. As can be seen in Table 4.3, to achieve similar results to IRE, 3463 V and 3757 V would need to be applied for the 10-1-10 and 5-1-5 H-FIRE waveforms respectively. These scaled voltages

achieved similar ablation surface areas, volumes, and sphericities to IRE; however, these voltages end up ablating more of the tumor specifically, achieving 91% ablation for 10-1-10, and 92.4% ablation for 5-1-5. The tunability of parameters based off the electric field distribution in the 2D axisymmetric model, and the ablation and sphericity quantifications from the 3D model, demonstrate the potential of H-FIRE to achieve comparable ablation results to that of IRE with fine-tuned treatment parameters.

Table 4.2: Ablation quantification and sphericity calculations of all pulsing schemes at the maximum clinical voltage of 3000 V.

Variable	5-1-5	10-1-10	IRE
Ablation Surface Area (A, cm^2)	28.567	34.270	37.437
Tumor Ablation Volume (V1, cm^3)	7.0347	9.284	12.371
Entire Ablation Volume (V2, cm^3)	8.3530	11.370	15.905
Sphericity (V1)	0.6215	0.6233	0.6909
Sphericity (V2)	0.6969	0.7135	0.8169

Table 4.3: Ablation quantification and sphericity calculation of H-FIRE waveforms with scaled voltages to achieve comparable IRE results.

Variable	5-1-5 (3757 V)	10-1-10 (3463 V)	IRE (3000 V)
Ablation Surface Area (A, cm^2)	39.238	38.734	37.437
Tumor Ablation Volume (V1, cm^3)	13.064	12.872	12.371
Entire Ablation Volume (V2, cm^3)	17.074	16.744	15.905
Sphericity (V1)	0.6836	0.6857	0.6969
Sphericity (V2)	0.8172	0.8171	0.8196

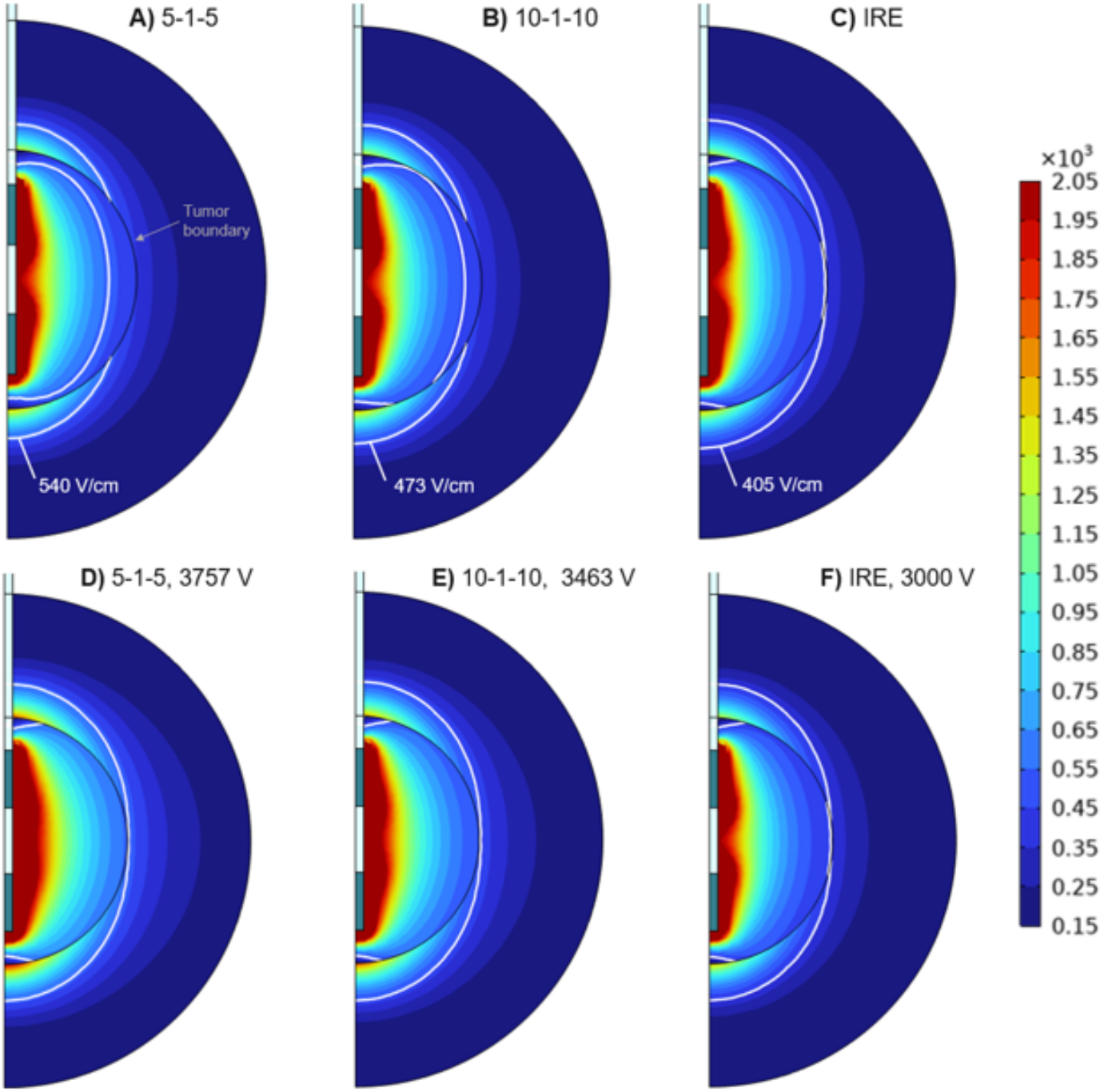

Figure 4.4: (A-C) Electric field distribution travels farther out into the peripheral tissue for IRE than the H-FIRE waveforms at 3000 V. (D-F) Electric field distribution with scaled H-FIRE voltages. White contour lines on each plot mark the specific EFT for each waveform. The black semicircle in the middle demarcates the tumor boundary (r=1.5 cm).

4.5 Discussion and Conclusion

Figure 4.4 demonstrates the potential of tuned H-FIRE parameters to ablate the same quantity of breast tumor as IRE. Quite unexpectedly, 5-1-5 ended up ablating a larger percentage of the tumor, but this can be explained by the much higher applied voltages compared to 10-1-10 and IRE. Although not included in this thesis document, an important consideration that must be reflected in further modeling is the potential thermal damage that may result from the very high voltages. It is unclear to what extent we expect thermal damage to occur, but further fine-tuning of treatment parameters may facilitate reducing potential thermal damage. For instance, increasing the interpulse delay may result in reducing heat produced from the waveform [8], as well as utilizing a different electrode configuration based off patient-specific tumor dimensions.

One of the most important aspects of delivering electroporation in the clinic is performing accurate treatment planning beforehand. The generated models in this project were run in the dynamic module, which takes into account changes in temperature and conductivity over time. The static module can also be used to run these models; however, this will only show us immediate electroporation effects. Using accurate treatment planning we can also visualize the shape of the ablation in relation to the shape of the tumor to see what parameters achieve the greatest tumor coverage. One of the benefits of H-FIRE is the generation of a more consistent electric field distribution and predictable ablation shape. Treatment planning allows us to input patient-specific tumor dimensions, typically from MRI images and compare ablation coverage with various treatment parameter scenarios. The representative electric field distributions using the single bipolar probe would change depending on the depth of probe insertion; therefore, clinicians may need to utilize real-time imaging (i.e. ultrasound guidance) be sure of accurate placement of electrodes. As is the case for most tumors, a breast tumor will have a higher conductivity that the peripheral healthy tissue

likely due to the regions of necrotic tissue that no longer have the insulating cellular membrane. Since electric field distribution is dependent on the conductivity ratio of tumor and healthy tissue (as well as electrode geometry), tissue characterization experiments should be performed to collect relevant data for breast tumors and the heterogeneous peripheral tissue. Additionally, the lethal EFTs treated as E_{del} values for modeling dynamic changes in conductivity were found for a malignant breast cell line. To have EFT data representative of the healthy peripheral tissue, hydrogel experiments should be performed with a non-malignant breast cell line and used to update the model. Even though obtaining these values would provide a more comprehensive breast tumor model, these EFT values are assumed to not be fully representative of true electroporation treatments, as *in vivo* EFTs will be higher than *in vitro* due to the effect of cell size on electric field as explained in Section 2.1.

Chapter 5

Thesis Conclusions

The goal of this project was to provide sufficient fundamental knowledge and insight into using H-FIRE as a stand-alone therapy for BC. Although comparing MDA-MB-231 and MCF-7 cells gives us a better understanding of the response of BC to EP treatment, further research needs to be conducted to better represent the heterogeneity that exists in BC. Furthermore, the underlying explanation as to why the MDA-MB-231 cells were not compatible in the collagen hydrogel remains a mystery. While it may require a collaborative effort to determine this, finding a compatible treatment platform would enhance our understanding of H-FIRE in a triple-negative phenotype specifically. The next step in this project is to repeat hydrogel experiments with the MDA-MB-231 cells at a lower confluency to see if this explains the unexpected results, as well as with a non-cancerous human breast cell line like MCF-10A to draw comparisons between healthy and malignant tissues and see how neighboring cells may succumb to electroporation effects.

A very important engineering consideration for accurate electroporation treatment is that of dynamic conductivity from tissue characterization, which was not included in this thesis project. Fourier transforms can aid in electrical properties from characterizing tissue samples. This process allows us to find baseline conductivity values in a tissue type after a specific treatment waveform has been applied. To achieve these values for this project in the future, healthy breast tissue would need to be collected from each type of tissue (glands, ducts, adipose fat), as well as a biopsy from a breast tumor that would all be kept in buffer

solution to maintain the same electrical properties they possess in the body. Various frequencies can be applied to characterize tissue impedance values and electric field threshold that can be implemented in COMSOL for accurate treatment planning and outcome.

In the future, there are numerous possibilities to improve upon this study. One idea would be to add calcium (Ca^{2+}) directly to the cell media or buffer solution to see if there is an increase in ablation volume, as this has been proven before in treating glioblastoma with IRE [95] and malignant glioma with H-FIRE [96]. Although very preliminary, it would be interesting to note the differences between pulse number in ablation size, as 100 pulses were kept constant for all experiments. While this is a standard clinical delivery amount, burst number will change the resulting EFT. Therefore, researchers should have appropriate rationale when deciding treatment factors such as burst number. Adding a comparative study between cancerous and non-cancerous breast cell lines would aid in tissue characterization since malignant cells have a higher conductivity than that in non-cancerous cells. Another experiment could be done to test pulse parameters for cell death mechanism selectivity, and see if it's possible to provoke a specific mode, preferably pro-inflammatory for BC (i.e. pyroptosis). Pyroptosis is mediated by Gasdermin proteins, which are increasingly expressed in BC [22]. This could be done by studying cleaved proteins specific to pyroptosis activation like caspase 1 in the canonical pathway and caspase 4/5 in the non-canonical pathway. All of this *in vitro* information would prove useful for understanding the complexity of EP treatment for BC, and motivate *in vivo* experimentation. With the help of collaborators, human or murine BC cells could be injected into rats as these rodents' mammary glands are more similar to that of humans [58]. An experimental matrix would be designed to outline treatments groups to study H-FIRE, chemotherapy, and the combination of the two to study effect on tumor reduction and survival. Another collaborative project could be done to study the role of an important bacteria associated with poor treatment outcome, *Fusobacterium nucleatum*, and its role in the breast tumor microbiome [73].

In summation, the *in vitro* hydrogel experiments and numerical modeling conducted in this thesis proves our expectations that IRE would generate desirable ablation results. However, it should not be considered the best treatment option for clinical BC applications because of the requirement for general anesthesia for mitigating neuromuscular contractions. Due to these drawbacks, it was our goal that we'd be able to generate equivalent or preferable results with H-FIRE, which was also proven from the work done in Chapters 3 and 4. Therefore, the condensed work of this thesis proves that H-FIRE would be feasible as an alternative BC treatment, and with further experimentation it could hopefully become a standard treatment option. However, additional research is warranted in the future to fine-tune treatment parameters for understanding expected outcomes.

Bibliography

[1] IT'IS Foundation Dielectric Properties. URL https://itis.swiss/virtual-population/tissue-properties/database/dielectric-properties/.

[2] Incidence and relative survival by stage at diagnosis for common cancers, Nov 2021. URL https://www.cdc.gov/cancer/uscs/about/data-briefs/no25-incidence-relative-survival-stage-diagnosis.htm.

[3] ACS. Chemotherapy side effects, May 2020. URL https://www.cancer.org/treatment/treatments-and-side-effects/treatment-types/chemotherapy/chemotherapy-side-effects.html.

[4] ACS. Breast cancer statistics: How common is breast cancer?, Jan 2023. URL https://www.cancer.org/cancer/breast-cancer/about/how-common-is-breast-cancer.html#:~:text=It%20is%20about%2030%25%20.

[5] Christopher B Arena, Michael B Sano, John H Rossmeisl, John L Caldwell, Paulo A Garcia, Marissa Nichole Rylander, and Rafael V Davalos. High-frequency irreversible electroporation (h-fire) for non-thermal ablation without muscle contraction. *Biomedical engineering online*, 10(1):1–21, 2011.

[6] Christopher B Arena, Christopher S Szot, Paulo A Garcia, Marissa Nichole Rylander, and Rafael V Davalos. A three-dimensional in vitro tumor platform for modeling therapeutic irreversible electroporation. *Biophysical journal*, 103(9):2033–2042, 2012.

[7] Kenneth N Aycock and Rafael V Davalos. Irreversible electroporation: background,

theory, and review of recent developments in clinical oncology. *Bioelectricity*, 1(4): 214–234, 2019.

[8] Kenneth N Aycock, Yajun Zhao, Melvin F Lorenzo, and Rafael V Davalos. A theoretical argument for extended interpulse delays in therapeutic high-frequency irreversible electroporation treatments. *IEEE Transactions on Biomedical Engineering*, 68(6): 1999–2010, 2021.

[9] Kenneth N Aycock, Sabrina N Campelo, and Rafael V Davalos. A comparative modeling study of thermal mitigation strategies in irreversible electroporation treatments. *Journal of heat transfer*, 144(3):031206, 2022.

[10] Gholamhossein Bagheri and Costanza Bonadonna. Aerodynamics of volcanic particles: characterization of size, shape, and settling velocity. In *Volcanic ash*, pages 39–52. Elsevier, 2016.

[11] Bruce C Baguley and Euphemia Leung. Heterogeneity of phenotype in breast cancer cell lines. *Breast Cancer-Carcinogenesis, Cell Growth and Signalling Pathways*, pages 245–256, 2011.

[12] Christopher Bastianpillai, Neophytos Petrides, Taimur Shah, Stephanie Guillaumier, Hashim U Ahmed, and Manit Arya. Harnessing the immunomodulatory effect of thermal and non-thermal ablative therapies for cancer treatment. *Tumor Biology*, 36: 9137–9146, 2015.

[13] Ulrike Benbow, Matthias P Schoenermark, Kenneth A Orndorff, Alice L Givan, and Constance E Brinckerhoff. Human breast cancer cells activate procollagenase-1 and invade type i collagen: invasion is inhibited by all-trans retinoic acid. *Clinical & experimental metastasis*, 17:231–238, 1999.

[14] Suyashree Bhonsle, Mohammad Bonakdar, Robert E Neal II, Charles Aardema, John L Robertson, Jonathon Howarth, Helen Kavnoudias, Kenneth R Thomson, S Nahum Goldberg, and Rafael V Davalos. Characterization of irreversible electroporation ablation with a validated perfused organ model. *Journal of Vascular and Interventional Radiology*, 27(12):1913–1922, 2016.

[15] Suyashree P Bhonsle, Christopher B Arena, Daniel C Sweeney, and Rafael V Davalos. Mitigation of impedance changes due to electroporation therapy using bursts of high-frequency bipolar pulses. *Biomedical engineering online*, 14(3):1–14, 2015.

[16] Mohammad Bonakdar, Elisa M Wasson, Yong W Lee, and Rafael V Davalos. Electroporation of brain endothelial cells on chip toward permeabilizing the blood-brain barrier. *Biophysical journal*, 110(2):503–513, 2016.

[17] L Bracci, G Schiavoni, A Sistigu, and F Belardelli. Immune-based mechanisms of cytotoxic chemotherapy: implications for the design of novel and rationale-based combined treatments against cancer. *Cell Death & Differentiation*, 21(1):15–25, 2014.

[18] Ruggero Cadossi, Mattia Ronchetti, and Matteo Cadossi. Locally enhanced chemotherapy by electroporation: clinical experiences and perspective of use of electrochemotherapy. *Future Oncology*, 10(5):877–890, 2014.

[19] Sabrina N Campelo, Po-Hsun Huang, Cullen R Buie, and Rafael V Davalos. Recent advancements in electroporation technologies: From bench to clinic. *Annual Review of Biomedical Engineering*, 25, 2022.

[20] CDC. Breast cancer, Sep 2022. URL https://www.cdc.gov/cancer/breast/index.htm.

[21] Arjun Chanmugam, Rajeev Hatwar, and Cila Herman. Thermal analysis of cancerous

breast model. In *ASME International Mechanical Engineering Congress and Exposition*, volume 45189, pages 135–143. American Society of Mechanical Engineers, 2012.

[22] Cong Chen, Qianwei Ye, Linbo Wang, Jichun Zhou, Aizhai Xiang, Xia Lin, Jufeng Guo, Shufang Hu, Tao Rui, and Jian Liu. Targeting pyroptosis in breast cancer: biological functions and therapeutic potentials on it. *Cell Death Discovery*, 9(1):75, 2023.

[23] Selma Corovic, Igor Lackovic, Primoz Sustaric, Tomaz Sustar, Tomaz Rodic, and Damijan Miklavcic. Modeling of electric field distribution in tissues during electroporation. *Biomedical engineering online*, 12:1–27, 2013.

[24] Rafael V Davalos and Boris Rubinsky. Temperature considerations during irreversible electroporation. *International journal of heat and mass transfer*, 51(23-24):5617–5622, 2008.

[25] Rafael V Davalos, LM Mir, and B Rubinsky. Tissue ablation with irreversible electroporation. *Annals of biomedical engineering*, 33:223–231, 2005.

[26] Rafael V Davalos, Paulo A Garcia, and Jon F Edd. Thermal aspects of irreversible electroporation. *Irreversible Electroporation*, pages 123–154, 2010.

[27] Rafael V Davalos, Suyashree Bhonsle, and Robert E Neal. Implications and considerations of thermal effects when applying irreversible electroporation tissue ablation therapy. *The Prostate*, 75(10):1114–1118, 2015.

[28] Tim C de Ruijter, Jürgen Veeck, Joep PJ de Hoon, Manon van Engeland, and Vivianne C Tjan-Heijnen. Characteristics of triple-negative breast cancer. *Journal of cancer research and clinical oncology*, 137:183–192, 2011.

[29] Katherine A DeBruin and Wanda Krassowska. Modeling electroporation in a single

cell. i. effects of field strength and rest potential. *Biophysical journal*, 77(3):1213–1224, 1999.

[30] Petra Den Hollander, Michelle I Savage, and Powel H Brown. Targeted therapy for breast cancer prevention. *Frontiers in oncology*, 3:250, 2013.

[31] Matthew R DeWitt, Eduardo L Latouche, Jacob D Kaufman, Christopher C Fesmire, Jacob H Swet, Russel C Kirks, Erin H Baker, Dionisios Vrochides, David A Iannitti, Iain H McKillop, et al. Simplified non-thermal tissue ablation with a single insertion device enabled by bipolar high-frequency pulses. *IEEE Transactions on Biomedical Engineering*, 67(7):2043–2051, 2019.

[32] Mihajlo Djokic, Maja Cemazar, Miha Stabuc, Miha Petric, Lojze M Smid, Rado Jansa, Bostjan Plesnik, Masa Bosnjak, Ursa Lampreht Tratar, Blaz Trotovsek, et al. Percutaneous image guided electrochemotherapy of hepatocellular carcinoma: technological advancement. *Radiology and Oncology*, 54(3):347–352, 2020.

[33] Shoulong Dong, Haifeng Wang, Yajun Zhao, Yinghao Sun, and Chenguo Yao. First human trial of high-frequency irreversible electroporation therapy for prostate cancer. *Technology in cancer research & treatment*, 17:1533033818789692, 2018.

[34] Jon F Edd and Rafael V Davalos. Mathematical modeling of irreversible electroporation for treatment planning. *Technology in cancer research & treatment*, 6(4):275–286, 2007.

[35] Loreto B Feril, Rodney L Fernan, and Katsuro Tachibana. High-intensity focused ultrasound in the treatment of breast cancer. *Current Medicinal Chemistry*, 28(25): 5179–5188, 2021.

[36] Xiaoyu Fu, Wei Tan, Qibin Song, Huadong Pei, and Juanjuan Li. Brca1 and breast

cancer: molecular mechanisms and therapeutic strategies. *Frontiers in cell and developmental biology*, 10, 2022.

[37] Paulo A Garcia, Rafael V Davalos, and Damijan Miklavcic. A numerical investigation of the electric and thermal cell kill distributions in electroporation-based therapies in tissue. *PloS one*, 9(8):e103083, 2014.

[38] Paulo A Garcia, Rafael V Davalos, and Damijan Miklavcic. A numerical investigation of the electric and thermal cell kill distributions in electroporation-based therapies in tissue. *PloS one*, 9(8):e103083, 2014.

[39] Bart Geboers, Hester J Scheffer, Philip M Graybill, Alette H Ruarus, Sanne Nieuwenhuizen, Robbert S Puijk, Petrousjka M van den Tol, Rafael V Davalos, Boris Rubinsky, Tanja D de Gruijl, et al. High-voltage electrical pulses in oncology: irreversible electroporation, electrochemotherapy, gene electrotransfer, electrofusion, and electroimmunotherapy. *Radiology*, 295(2):254–272, 2020.

[40] Pragatheiswar Giri, Ignacio G Camarillo, Lakshaya Mitta, and Raji Sundararajan. Quantitative proteomic assessment of key proteins regulated by electrical pulse-mediated galloflavin delivery in triple-negative breast cancer cells. *Biointerface Research in Applied Chemistry*, 2022.

[41] Pragatheiswar Giri, Ignacio G Camarillo, and Raji Sundararajan. Enhanced induction of mda-mb-231 cell death using the combination of galloflavin and electroporation. *Biointerface Research in Applied Chemistry*, 2022.

[42] Ishan Goswami, Sheryl Coutermarsh-Ott, Ryan G Morrison, Irving C Allen, Rafael V Davalos, Scott S Verbridge, and Lissett R Bickford. Irreversible electroporation inhibits pro-cancer inflammatory signaling in triple negative breast cancer cells. *Bioelectrochemistry*, 113:42–50, 2017.

[43] E Guenther, N Klein, S Zapf, S Weil, C Schlosser, Boris Rubinsky, and MK Stehling. Prostate cancer treatment with irreversible electroporation (ire): Safety, efficacy and clinical experience in 471 treatments. *PloS one*, 14(4):e0215093, 2019.

[44] Ming-Jung Heish, Therese Salameh, Ignacio Camarillo, and Raji Sundararajan. Irreversible electroporation effects: A drug-free treatment for cancer. In *Proc. ESA Annual Meeting on Electrostatics*, volume 4, pages 1–7, 2011.

[45] Jill W Ivey, Eduardo L Latouche, Michael B Sano, John H Rossmeisl, Rafael V Davalos, and Scott S Verbridge. Targeted cellular ablation based on the morphology of malignant cells. *Scientific reports*, 5(1):17157, 2015.

[46] Francesco Izzo, Vincenza Granata, Roberta Fusco, Valeria D'Alessio, Antonella Petrillo, Secondo Lastoria, Mauro Piccirillo, Vittorio Albino, Andrea Belli, Salvatore Tafuto, et al. Clinical phase i/ii study: Local disease control and survival in locally advanced pancreatic cancer treated with electrochemotherapy. *Journal of Clinical Medicine*, 10(6):1305, 2021.

[47] Edward J Jacobs IV, Philip M Graybill, Aniket Jana, Atharva Agashe, Amrinder S Nain, and Rafael V Davalos. Engineering high post-electroporation viabilities and transfection efficiencies for elongated cells on suspended nanofiber networks. *Bioelectrochemistry*, 152:108415, 2023.

[48] Chunlan Jiang, Rafael V Davalos, and John C Bischof. A review of basic to clinical studies of irreversible electroporation therapy. *IEEE Transactions on biomedical Engineering*, 62(1):4–20, 2014.

[49] Chunlan Jiang, Zhenpeng Qin, and John Bischof. Membrane-targeting approaches for enhanced cancer cell destruction with irreversible electroporation. *Annals of biomedical engineering*, 42:193–204, 2014.

[50] William T Joines, Yang Zhang, Chenxing Li, and Randy L Jirtle. The measured electrical properties of normal and malignant human tissues from 50 to 900 mhz. *Medical physics*, 21(4):547–550, 1994.

[51] Natanel Jourabchi, Kourosh Beroukhim, Bashir A Tafti, Stephen T Kee, and Edward W Lee. Irreversible electroporation (nanoknife) in cancer treatment. *Gastrointestinal Intervention*, 3(1):8–18, 2014.

[52] Tadej Kotnik and Damijan Miklavčič. Theoretical evaluation of voltage inducement on internal membranes of biological cells exposed to electric fields. *Biophysical journal*, 90(2):480–491, 2006.

[53] Tadej Kotnik, Gorazd Pucihar, and Damijan Miklavčič. Induced transmembrane voltage and its correlation with electroporation-mediated molecular transport. *The Journal of membrane biology*, 236:3–13, 2010.

[54] Tadej Kotnik, Peter Kramar, Gorazd Pucihar, Damijan Miklavcic, and Mounir Tarek. Cell membrane electroporation-part 1: The phenomenon. *IEEE Electrical Insulation Magazine*, 28(5):14–23, 2012.

[55] Wanda Krassowska and Petar D Filev. Modeling electroporation in a single cell. *Biophysical journal*, 92(2):404–417, 2007.

[56] Xiaoxiang Li, Kui Xu, Wei Li, Xiuchun Qiu, Baoan Ma, Qingyu Fan, and Zhao Li. Immunologic response to tumor ablation with irreversible electroporation. *PloS one*, 7(11):e48749, 2012.

[57] JD Litster. Stability of lipid bilayers and red blood cell membranes. *Physics Letters A*, 53(3):193–194, 1975.

[58] Chong Liu, Pei Wu, Ailin Zhang, and Xiaoyun Mao. Advances in rodent models for breast cancer formation, progression, and therapeutic testing. *Frontiers in Oncology*, 11:593337, 2021.

[59] Melvin F Lorenzo, Sabrina N Campelo, Julio P Arroyo, Kenneth N Aycock, Jonathan Hinckley, Christopher B Arena, John H Rossmeisl Jr, and Rafael V Davalos. An investigation for large volume, focal blood-brain barrier disruption with high-frequency pulsed electric fields. *Pharmaceuticals*, 14(12):1333, 2021.

[60] Damijan Miklavčič, Barbara Mali, Bor Kos, Richard Heller, and Gregor Serša. Electrochemotherapy: from the drawing board into medical practice. *Biomedical engineering online*, 13:1–20, 2014.

[61] Kelsey R Murphy, aycockth N Aycock, Alayna N Hay, John H Rossmeisl, Rafael V Davalos, and Nikolaos G Dervisis. High-frequency irreversible electroporation brain tumor ablation: exploring the dynamics of cell death and recovery. *Bioelectrochemistry*, 144:108001, 2022.

[62] RE Neal, JH Rossmeisl, V D'alfonso, JL Robertson, PA Garcia, S Elankumaran, and RV Davalos. In vitro and numerical support for combinatorial irreversible electroporation and electrochemotherapy glioma treatment. *Annals of biomedical engineering*, 42:475–487, 2014.

[63] Robert E Neal and Rafael V Davalos. The feasibility of irreversible electroporation for the treatment of breast cancer and other heterogeneous systems. *Annals of biomedical engineering*, 37:2615–2625, 2009.

[64] Robert E Neal, Ravi Singh, Heather C Hatcher, Nancy D Kock, Suzy V Torti, and Rafael V Davalos. Treatment of breast cancer through the application of irreversible

electroporation using a novel minimally invasive single needle electrode. *Breast cancer research and treatment*, 123:295–301, 2010.

[65] Robert E Neal, Paulo A Garcia, Helen Kavnoudias, Franklin Rosenfeldt, Catriona A Mclean, Victoria Earl, Joanne Bergman, Rafael V Davalos, and Kenneth R Thomson. In vivo irreversible electroporation kidney ablation: experimentally correlated numerical models. *IEEE Transactions on Biomedical Engineering*, 62(2):561–569, 2014.

[66] Robert E Neal, Jeremy L Millar, Helen Kavnoudias, Peter Royce, Franklin Rosenfeldt, Alan Pham, Ryan Smith, Rafael V Davalos, and Kenneth R Thomson. In vivo characterization and numerical simulation of prostate properties for non-thermal irreversible electroporation ablation. *The Prostate*, 74(5):458–468, 2014.

[67] Eberhard Neumann and Kurt Rosenheck. Permeability changes induced by electric impulses in vesicular membranes. *The Journal of membrane biology*, 10(1):279–290, 1972.

[68] Tiffany Nguyen, Eleanor Hattery, and Vijay P Khatri. Radiofrequency ablation and breast cancer: a review. *Gland surgery*, 3(2):128, 2014.

[69] NIH. Radiation therapy side effects, Jan 2023. URL https://www.cancer.gov/about-cancer/treatment/types/radiation-therapy/side-effects.

[70] Timothy J O'Brien, Mohammad Bonakdar, Suyashree Bhonsle, Robert E Neal, Charles H Aardema Jr, John L Robertson, S Nahum Goldberg, and Rafael V Davalos. Effects of internal electrode cooling on irreversible electroporation using a perfused organ model. *International Journal of Hyperthermia*, 35(1):44–55, 2018.

[71] Timothy J O'Brien, Melvin F Lorenzo, Yajun Zhao, Robert E Neal II, John L Robertson, S Nahum Goldberg, and Rafael V Davalos. Cycled pulsing to mitigate thermal

damage for multi-electrode irreversible electroporation therapy. *International Journal of Hyperthermia*, 36(1):952–962, 2019.

[72] Timothy J O'Brien, Michael Passeri, Melvin F Lorenzo, Jesse K Sulzer, William B Lyman, Jacob H Swet, Dionisios Vrochides, Erin H Baker, David A Iannitti, Rafael V Davalos, et al. Experimental high-frequency irreversible electroporation using a single-needle delivery approach for nonthermal pancreatic ablation in vivo. *Journal of Vascular and Interventional Radiology*, 30(6):854–862, 2019.

[73] Lishay Parhi, Tamar Alon-Maimon, Asaf Sol, Deborah Nejman, Amjad Shhadeh, Tanya Fainsod-Levi, Olga Yajuk, Batya Isaacson, Jawad Abed, Naseem Maalouf, et al. Breast cancer colonization by fusobacterium nucleatum accelerates tumor growth and metastatic progression. *Nature communications*, 11(1):3259, 2020.

[74] MCL Peek, M Ahmed, A Napoli, Bernard ten Haken, S McWilliams, SI Usiskin, SE Pinder, M Van Hemelrijck, and Michael Douek. Systematic review of high-intensity focused ultrasound ablation in the treatment of breast cancer. *Journal of British Surgery*, 102(8):873–882, 2015.

[75] Mirjam CL Peek and Michael Douek. Ablative techniques for the treatment of benign and malignant breast tumours. *Journal of therapeutic ultrasound*, 5(1):1–7, 2017.

[76] Kevin T Powell and James C Weaver. Transient aqueous pores in bilayer membranes: a statistical theory. *Bioelectrochemistry and Bioenergetics*, 15(2):211–227, 1986.

[77] Vishak Raman, Ignacio Camarillo, Allen Garner, Prasoon Diwakar, S Madhivanan, M Raakesh, and Raji Sundararajan. Irreversible electroporation of aggressive triple-negative breast cancer cells. In *2015 IEEE Conference on Electrical Insulation and Dielectric Phenomena (CEIDP)*, pages 624–627. IEEE, 2015.

[78] Vivek Y Reddy, Jacob Koruth, Pierre Jais, Jan Petru, Ferdinand Timko, Ivo Skalsky, Robert Hebeler, Louis Labrousse, Laurent Barandon, Stepan Kralovec, et al. Ablation of atrial fibrillation with pulsed electric fields: an ultra-rapid, tissue-selective modality for cardiac ablation. *JACC: Clinical Electrophysiology*, 4(8):987–995, 2018.

[79] Veronica M Ringel-Scaia, Natalie Beitel-White, Melvin F Lorenzo, Rebecca M Brock, Kathleen E Huie, Sheryl Coutermarsh-Ott, Kristin Eden, Dylan K McDaniel, Scott S Verbridge, John H Rossmeisl, et al. High-frequency irreversible electroporation is an effective tumor ablation strategy that induces immunologic cell death and promotes systemic anti-tumor immunity. *EBioMedicine*, 44:112–125, 2019.

[80] John H Rossmeisl, Paulo A Garcia, Theresa E Pancotto, John L Robertson, Natalia Henao-Guerrero, Robert E Neal, Thomas L Ellis, and Rafael V Davalos. Safety and feasibility of the nanoknife system for irreversible electroporation ablative treatment of canine spontaneous intracranial gliomas. *Journal of neurosurgery*, 123(4):1008–1025, 2015.

[81] Leif G Salford, BRR Persson, Arne Brun, CP Ceberg, P Ch Kongstad, and Lluis M Mir. A new brain tumor therapy combining bleomycin with in vivo electropermeabilization. *Biochemical and biophysical research communications*, 194(2):938–943, 1993.

[82] Yara E Sánchez-Corrales, Matthew Hartley, Jop Van Rooij, Athanasius FM Marée, and Verônica A Grieneisen. Morphometrics of complex cell shapes: lobe contribution elliptic fourier analysis (loco-efa). *Development*, 145(6):dev156778, 2018.

[83] Arun Kumar Sharma and Archana Sharma. 5 - staining. In Arun Kumar Sharma and Archana Sharma, editors, *Chromosome Techniques (Third Edition)*, pages 91–139. Butterworth-Heinemann, third edition edition, 1980. ISBN 978-0-408-70942-

2. doi: https://doi.org/10.1016/B978-0-408-70942-2.50010-9. URL https://www.sciencedirect.com/science/article/pii/B9780408709422500109.

[84] Andrew Y Shuen and William D Foulkes. Inherited mutations in breast cancer genes—risk and response. *Journal of mammary gland biology and neoplasia*, 16:3–15, 2011.

[85] Imran A Siddiqui, Eduardo L Latouche, Matthew R DeWitt, Jacob H Swet, Russell C Kirks, Erin H Baker, David A Iannitti, Dionisios Vrochides, Rafael V Davalos, and Iain H McKillop. Induction of rapid, reproducible hepatic ablations using next-generation, high frequency irreversible electroporation (h-fire) in vivo. *Hpb*, 18(9): 726–734, 2016.

[86] Rebecca L Siegel, Kimberly D Miller, Hannah E Fuchs, and Ahmedin Jemal. Cancer statistics, 2022. *CA: a cancer journal for clinicians*, 72(1):7–33, 2022.

[87] R Stampfli. Reversible electrical breakdown of the excitable membrane of a ranvier node. *An Acad Brasil Ciens*, 30(1):57–61, 1958.

[88] Alan Sugrue, Vaibhav Vaidya, Chance Witt, Christopher V DeSimone, Omar Yasin, Elad Maor, Ammar M Killu, Suraj Kapa, Christopher J McLeod, Damijan Miklavčič, et al. Irreversible electroporation for catheter-based cardiac ablation: a systematic review of the preclinical experience. *Journal of Interventional Cardiac Electrophysiology*, 55:251–265, 2019.

[89] Andrzej J Surowiec, Stanislaw S Stuchly, J Robin Barr, and AASA Swarup. Dielectric properties of breast carcinoma and the surrounding tissues. *IEEE Transactions on Biomedical Engineering*, 35(4):257–263, 1988.

[90] Robert Susil, Dejan Šemrov, and Damijan Miklavčič. Electric field-induced transmem-

brane potential depends on cell density and organizatio. *Electro-and magnetobiology*, 17(3):391–399, 1998.

[91] Daniel C Sweeney, Robert E Neal, and Rafael V Davalos. Multi-scale biophysical principles in clinical irreversible electroporation. *Irreversible Electroporation in Clinical Practice*, pages 41–66, 2018.

[92] Christiane Taupin, Maya Dvolaitzky, and Claude Sauterey. Osmotic pressure-induced pores in phospholipid vesicles. *Biochemistry*, 14(21):4771–4775, 1975.

[93] Mehmet Toner and Ernest G Cravalho. Kinetics and likelihood of membrane rupture during electroporation. *Physics Letters A*, 143(8):409–412, 1990.

[94] Harold N. Trick and George W. Bates. *Electrofusion of Plant Protoplasts: Selection and Screening for Somatic Hybrids of Nicotiana*, volume 55, page 165–188. Humana Press, 1995.

[95] Elisa M Wasson, Jill W Ivey, Scott S Verbridge, and Rafael V Davalos. The feasibility of enhancing susceptibility of glioblastoma cells to ire using a calcium adjuvant. *Annals of biomedical engineering*, 45:2535–2547, 2017.

[96] Elisa M Wasson, Nastaran Alinezhadbalalami, Rebecca M Brock, Irving C Allen, Scott S Verbridge, and Rafael V Davalos. Understanding the role of calcium-mediated cell death in high-frequency irreversible electroporation. *Bioelectrochemistry*, 131: 107369, 2020.

[97] James C Weaver. Electroporation theory: concepts and mechanisms. *Plant cell electroporation and electrofusion protocols*, pages 3–28, 1995.

[98] James C Weaver and Yu A Chizmadzhev. Theory of electroporation: a review. *Bioelectrochemistry and bioenergetics*, 41(2):135–160, 1996.

[99] James C Weaver and Robert A Mintzer. Decreased bilayer stability due to transmembrane potentials. *Physics Letters A*, 86(1):57–59, 1981.

[100] Ozlem Yersal and Sabri Barutca. Biological subtypes of breast cancer: Prognostic and therapeutic implications. *World journal of clinical oncology*, 5(3):412, 2014.

[101] Jie Yu, Zhi-yu Han, Ting Li, Wen-zhe Feng, Xiao-ling Yu, Yan-chun Luo, Han Wu, Jian Jiang, Jian-dong Wang, and Ping Liang. Microwave ablation versus nipple sparing mastectomy for breast cancer 5 cm: a pilot cohort study. *Frontiers in Oncology*, 10: 546883, 2020.

[102] Sungryul Yu, Taemook Kim, Kyung Hyun Yoo, and Keunsoo Kang. The t47d cell line is an ideal experimental model to elucidate the progesterone-specific effects of a luminal a subtype of breast cancer. *Biochemical and Biophysical Research Communications*, 486(3):752–758, 2017.

[103] Yajun Zhao, Suyashree Bhonsle, Shoulong Dong, Yanpeng Lv, Hongmei Liu, Ahmad Safaai-Jazi, Rafael V Davalos, and Chenguo Yao. Characterization of conductivity changes during high-frequency irreversible electroporation for treatment planning. *IEEE Transactions on Biomedical Engineering*, 65(8):1810–1819, 2017.

[104] Yajun Zhao, Shuang Zheng, Natalie Beitel-White, Hongmei Liu, Chenguo Yao, and Rafael V Davalos. Development of a multi-pulse conductivity model for liver tissue treated with pulsed electric fields. *Frontiers in Bioengineering and Biotechnology*, 8: 396, 2020.

[105] Z Zhao and F Wu. Minimally-invasive thermal ablation of early-stage breast cancer: a systemic review. *European Journal of Surgical Oncology (EJSO)*, 36(12):1149–1155, 2010.

Appendices

Appendix A

First Appendix

A.1 Section one

Table A.1: Cell viability data found from cuvette experiments. In all H-FIRE waveforms, there is an inter-pulse delay of 1. For all applied waveforns, 100 bursts was used. The first and second row of field strengths correspond to Figure 3.5A and Figure 3.5B, respectively.

Parameters	Viability Results (%)			
Waveform / Electric Field Strength (V/cm)	2-1-2	5-1-5	10-1-10	IRE
0	108.07, 99.26, 92.65	107.50, 88.22, 104.27	115.00, 96.56, 88.43	111.81, 93.15, 95.02
750	96.97, 88.48, 97.65	77.07, 80.47, 77.24	88.60, 76.73, 60.15	65.60, 58.07, 87.34
1500	74.19, 75.06, 73.01	26.14, 25.72, 25.53	29.62, 27.83, 29.15	22.28, 21.85, 20.37
2250	22.28, 23.84, 25.28	25.91, 25.76, 27.63	25.95, 25.99, 28.29	16.63, 16.08, 19.76
3000	21.52, 19.92, 20.64	23.32, 20.74, 20.63	24.99, 23.37, 22.25	13.44, 12.08, 11.70
1250	80.72, 53.37, 50.32	17.90, 15.97, 17.38	6.61, 7.12, 10.32	2.62, 2.69, 2.99
1500	29.21, 28.15, 30.85	5.47, 5.20, 5.79	3.59, 3.25, 4.19	1.97, 1.90, 2.94
1750	13.94, 12.80, 12.83	2.58, 2.63, 2.74	2.52, 2.32, 2.38	3.13, 2.97, 3.05
2000	5.66, 6.88, 4.43	2.02, 2.25, 3.90	2.04, 1.66, 2.79	2.60, 2.24, 3.22
2250	3.21, 3.59, 3.52	2.62, 1.54, 2.15	2.17, 1.89, 1.90	2.90, 3.23, 4.17